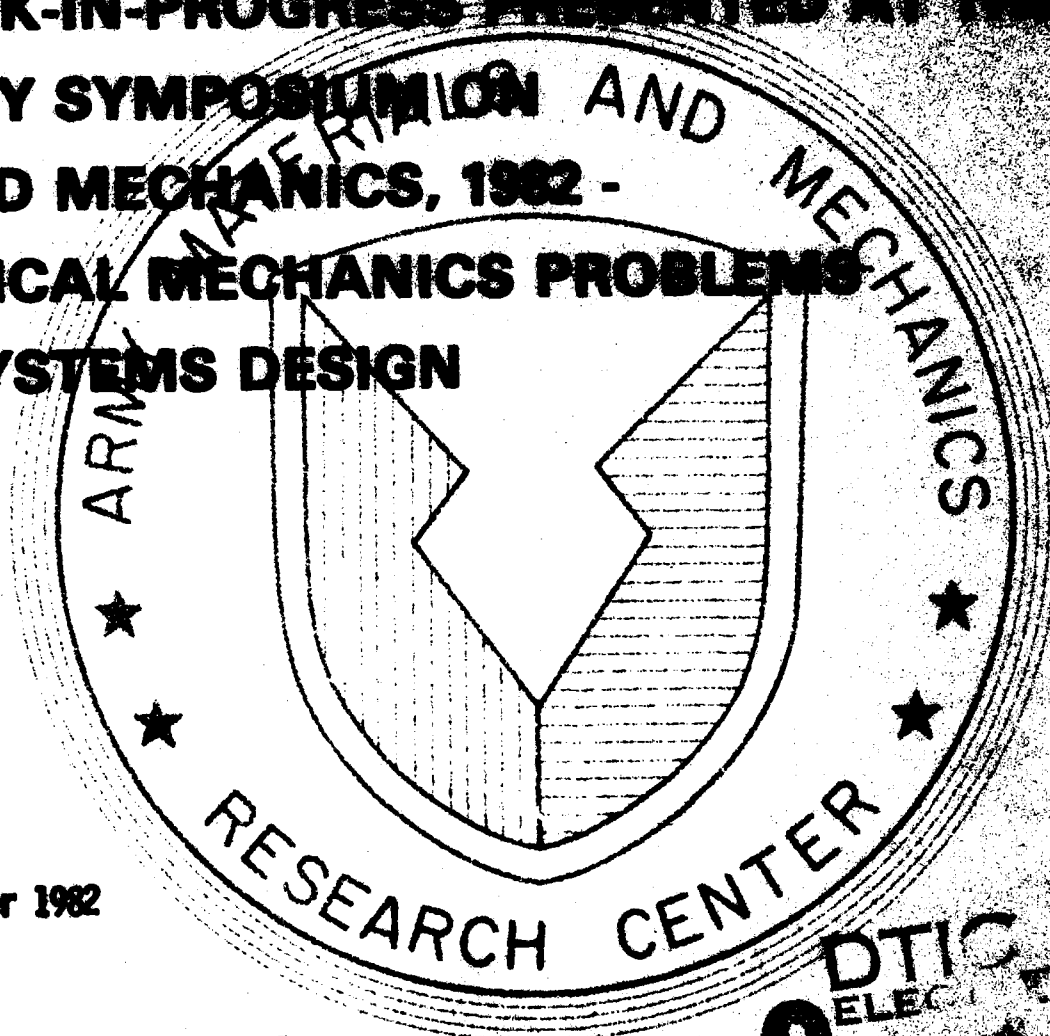END
DATE
FILMED
11 .82
DTIC

AMMRC MS 82-5

AD

WORK-IN-PROGRESS PRESENTED AT THE ARMY SYMPOSIUM ON SOLID MECHANICS, 1982 - CRITICAL MECHANICS PROBLEMS IN SYSTEMS DESIGN

September 1982

DTIC
SELECT
SEP 23 1982

A

Approved for public release; distribution unlimited.

ARMY MATERIALS AND MECHANICS RESEARCH CENTER
Watertown, Massachusetts 02172

82 09 23 005

REPORT DOCUMENTATION PAGE		READ INSTRUCTIONS BEFORE COMPLETING FORM
1. REPORT NUMBER AMMRC MS 82-5	2. GOVT ACCESSION NO. AD-A119497	3. RECIPIENT'S CATALOG NUMBER
4. TITLE (and Subtitle) Work-In-Progress presented at the Army Symposium on Solid Mechanics, 1982 - Critical Mechanics Problems in Systems Design		5. TYPE OF REPORT & PERIOD COVERED Final Report
		6. PERFORMING ORG. REPORT NUMBER
7. AUTHOR(s)		8. CONTRACT OR GRANT NUMBER(s)
9. PERFORMING ORGANIZATION NAME AND ADDRESS Army Materials and Mechanics Research Center Watertown, Massachusetts 02172 ATTN: DRXMR-S		10. PROGRAM ELEMENT, PROJECT, TASK AREA & WORK UNIT NUMBERS
11. CONTROLLING OFFICE NAME AND ADDRESS US Army Materiel Development and Readiness Command, Alexandria, VA 22333		12. REPORT DATE September 1982
		13. NUMBER OF PAGES
14. MONITORING AGENCY NAME & ADDRESS(if different from Controlling Office)		15. SECURITY CLASS. (of this report) Unclassified
		15a. DECLASSIFICATION/DOWNGRADING SCHEDULE

16. DISTRIBUTION STATEMENT (of this Report)

Approved for public release; distribution unlimited.

17. DISTRIBUTION STATEMENT (of the abstract entered in Block 20, if different from Report)

18. SUPPLEMENTARY NOTES

19. KEY WORDS (Continue on reverse side if necessary and identify by block number)

Ballistics	Fatigue	Mechanical Properties
Engineering	Impact	Mechanics
Failure (Mechanics)	Ordnance	Shock

20. ABSTRACT (Continue on reverse side if necessary and identify by block number)

Work-In-Progess presented at the Army Symposium on Solid Mechanics, 1982 - Critical Mechanics Problems in Systems Design, held at Bass River, Cape Cod Massachusetts, September 21-23, 1982.
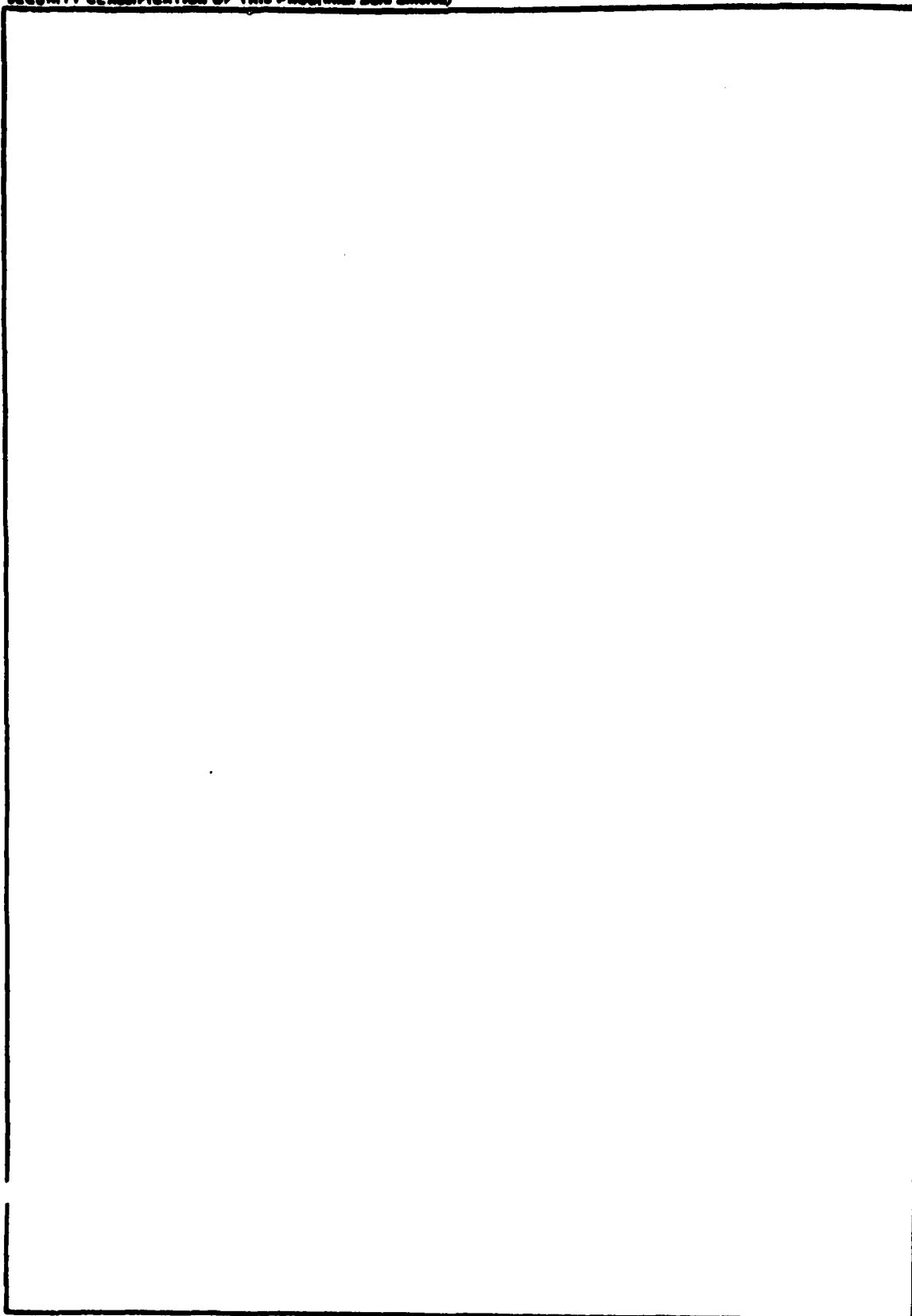
DD FORM 1473 EDITION OF 1 NOV 65 IS OBSOLETE
1 JAN 73

PREFACE

This document contains extended abstracts of presentations made within the Work-In-Progress Sessions of the Army Symposium on Solid Mechanics, 1982. These sessions were comprised of a series of brief presentations and discussions of current (but not necessarily complete) research relating to the theme of the conference: "Critical Mechanics Problems in Systems Design." This meeting was held at Bass River, Cape Cod, Massachusetts on 21-23 September 1982.

The proceedings of this symposium are published in a companion document, Army Materials and Mechanics Research Center, Manuscript Series Report: AMMRC MS 82-4, dated September 1982. The transactions of earlier symposia are listed on page iv of this document.

We acknowledge the contributions of the authors cited in the table of contents and also the staff of the Technical Reports Office of the Army Materials and Mechanics Research Center for their unflagging efforts in the preparation and printing of numerous symposium materials.

iii

---

*   These documents may be ordered from the National Technical Information
    Service, U.S. Department of Commerce, Springfield, VA 22161

SYMPOSIUM COMMITTEE

E. M. LENOE, Chairman, AMMRC
J. F. MESCALL, Vice Chairman, AMMRC
R. J. MORRISSEY, Secretary, AMMRC
J. M. AYOUB, Coordinator, AMMRC

TECHNICAL PAPERS AND PROGRAM

J. ADACHI, Chairman, AMMRC
A. A. ANCTIL, AMMRC
R. BARSOUM, AMMRC
L. BERKE, NASA-Lewis Research Center
C. I. CHANG, Naval Research Laboratory
H. D. CURCHACK, Harry Diamond Laboratories
C. M. ELDRIDGE, Army Missile command
J. FEROLI, Army Test and Evaluation Command
G. L. FILBEY, Jr., Ballistic Research Laboratories
R. FOYE, Army Aviation R&D Command
J. T. GARVIN, AMMRC
A. J. GUSTAFSON, Army Aviation R&D Command
H. HATCH, AMMRC
G. E. MADDUX, Air Force Wright Aeronautical Labs
J. F. MESCALL, AMMRC
D. R. MULVILLE, Naval Research Laboratory
D. M. NEAL, AMMRC
D. W. OPLINGER, AMMRC
R. P. PAPIRNO, AMMRC
R. QUATTRONE, Army Construction R&E Lab
E. W. ROSS, Jr., Army Natick R&D Command
M. E. ROYLANCE, AMMRC
E. SAIBEL, Army Research Office
T. SIMKINS, Army Armament R&D Command
J. H. SMITH, National Bureau of Standards
D. M. TRACEY, AMMRC

WORK-IN-PROGRESS SESSIONS

G. E. MADDUX, Co-Chairman, Air Force Wright Aeronautical Labs
R. P. PAPIRNO, Co-Chairman, AMMRC

CONTENTS

---

*Not presented orally due to time limitations.

APPLICATION OF FAILURE ANALYSIS FOR ENHANCED RELIABILITY
OF M60 TANK - REPORT OF M60 TASK GROUP*

ROSHDY S. BARSOUM
Army Materials & Mechanics Research Center
Watertown, MA   02172

ABSTRACT

Some recent tests (see e.g. reference, 1 for a similar discussion) on overhauled M60 tanks indicated the need for an effective means of evaluating the remaining useful life of a restored M60 tank after overhaul. This approach should lead to an increase in the tanks reliability measured in mean miles between failures.

A task group* was established at AMMRC to look into this problem. The study included analytical (structural mechanics, and statistics), testing, quality assurance (QA), non-destructive examination (NDE) and metallurgical disciplines. The task group decided to concentrate its efforts on the track and suspension system as a vital problem affecting the tank's mobility and movement. Exploiting the talents of its members, the task group, would perform a detailed, NDE, failure analysis, material and metallurgical evaluation, and study QA design requirement, and overhaul procedures.

The task group obtained design and failure data from TACOM and test data from the manufacturers. Members of the task group then visited the manufacturing facilities, the overhaul depot and field test sites.

In this report we discuss the work performed on the main component of the suspension system, the torsion bars. Torsion bars in the tank are designed to be mainly subjected to torsional loads, however, actual loading is feared to have some other stress components. In the first phase of the failure analysis, a bar which failed in the field was obtained. Figure 1. The examinations performed on the bar were:

1. Magnetic flux examination of both parts of the failed bar, to determine any other cracks;

2. Chemical analysis to evaluate conformity with the standards;

3. Standard charpy specimens, for evaluating transition temperature;

4. Pre-cracked charpy to evaluate fracture toughness;

5. Tension test;

---

6. Short-rod fracture specimen for evaluating fracture toughness,

7. Rockwell hardness traverse.

8. Fractographic examination of fracture surface, (a) light microscopy Figure 2 and (b) SEM, to locate the origin of cracks and the extent of fatigue crack growth, and

9. Metallurgical Examination of Crystaline Structure in the gage and spline area.

In order to evaluate the stress state and stress intensity factor in the spline region, the problem was broken up into three components:

1. Bearing stresses. Figure 3 shows the contours of maximum stresses.

2. Torsional shear stresses between the teeth. This problem was solved by analogy of the St. Venant Torsion formulation, Ref. 2, with heat transfer equations. Figure 4 shows the mesh and boundary conditions used in the analogue heat transfer solution.

3. Torsional shear solution due to change in cross-section of a non-prismatic shaft. The Michell equations, Ref. 2, of the angle of twist were used in the analogy with the heat transfer solution.

Futher, statistical evaluation of the torsion bar fatigue test data were performed to study heat-to-heat variation, "A" and "B" allowable variations from year to year and to recommend further test requirements.

After all these studies are completed a life forcasting methodology (3) will be used. The approach will depend on the level of confidence in data, loadings and results, and ability to perform NDE method.

Acknowledgment: Contact stress analysis was performed by C. E. Freese.

References

1. GAO Report to the Congress, Jan. 29, 1980.

2. S. Timoshenko and J. N. Goodier "Theory of Elasticity" McGraws-Hill.

3. R. T. Lund, F. R. Tuler, and J. R. Elliott, "Life Forcasting as a Logistics Technque", AMMRC TR 82-2.

Figure 2 Fractograph showing origin of failure

Figure 1 Torsion bar arrow shows origin of failure

3

SEGMENT C (2-ELEMENT DISTRIBUTED)
MAX-STRESS

-30.000
-40.000
-50.000
30.000
10.000
.00000
.00000

$\frac{\partial T}{\partial \theta}$

$f(q)$

$g(T)$

$\frac{\partial T}{\partial \theta}$
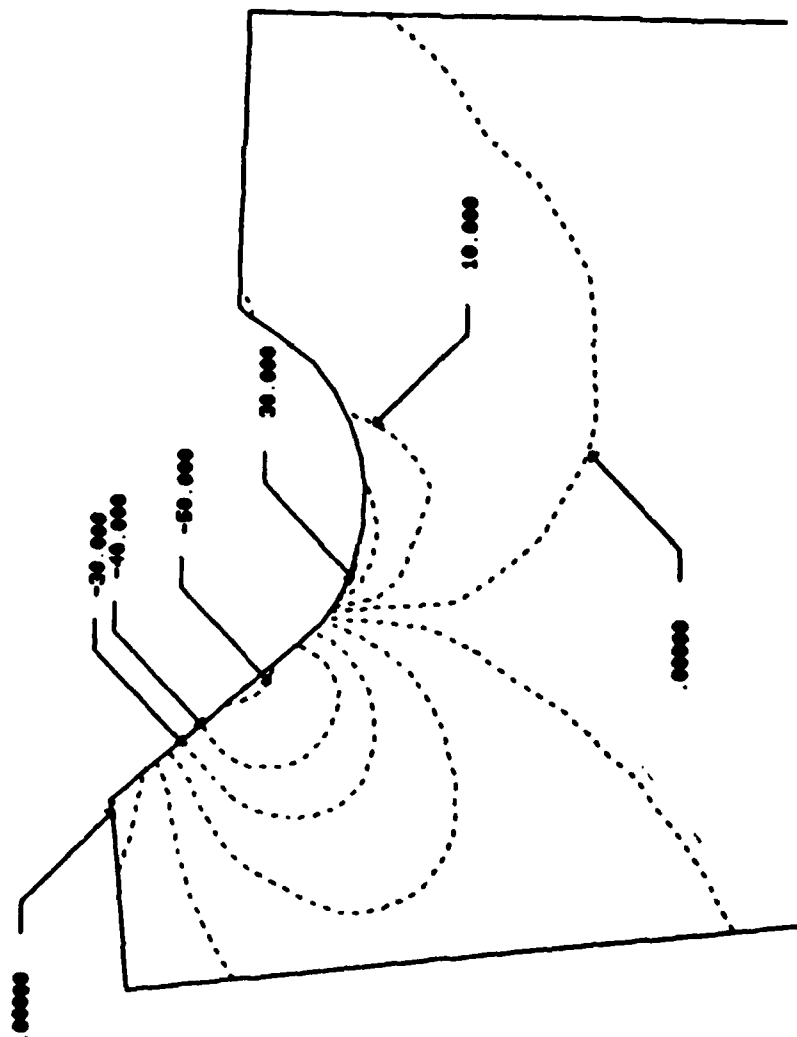
Figure 3 Maximum stresses from the Finite
Element analysis of Bearing stress
problem.
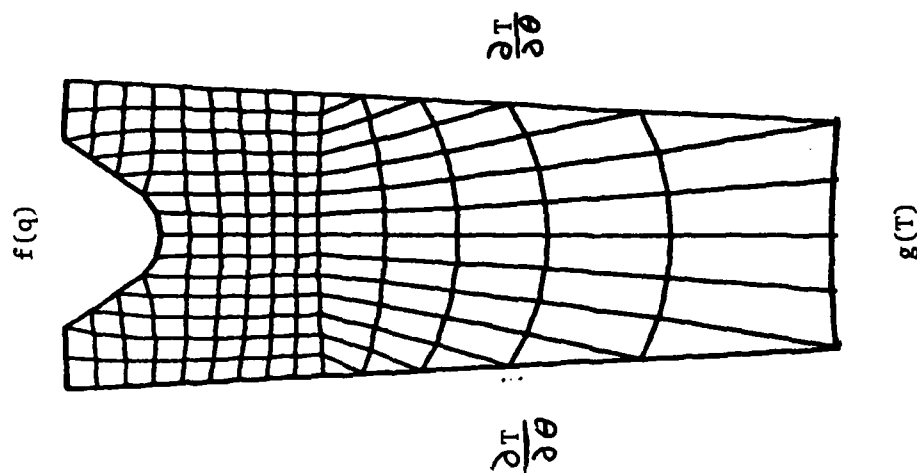
Figure 4 F. E. model for
Torsional stress Analysis
Heat Transf. Analogy

4

A COMPUTER PROGRAM FOR DAMAGE-TOLERANT OPTIMAL DESIGN OF COMPLEX STRUCTURES

D.T. NGUYEN
Department of Civil Engineering
Northeastern University
Boston, MA 02115

J.S. ARORA
A.D. BELEGUNDU
Division of Materials Engineering
The University of Iowa
Iowa City, IA 52242

EXTENDED ABSTRACT

During the last two decades considerable research has been done to develop optimization methods for design of structural systems. Benefits of the use of optimization techniques in the design process have been demonstrated. It is clear that with the use of optimization techniques, the practical design process can be accelerated and automated to some extent. However, research continues on development of new algorithms and testing of the existing algorithms to determine which of the methods is most suitable for structural optimization.

Whereas application of the optimization techniques for design of industrial products has appeared in the recent literature, the use of such techniques is not wide spread. One reason for the lack of this usage is that general purpose, well-tested computer codes are not available for design optimization of engineering systems. Some special purpose applications oriented computer programs have been developed. These include TRUSSOPT [1] and other programs [2,3]. These programs have been used successfully to optimize specific classes of structural design problems. What is needed is general purpose design-oriented software that can treat a variety of design environments. To develop such a capability one needs to integrate existing structural analysis programs into optimization algorithms to develop a general and user-oriented software for structural optimization. Some progress has been made in this regard [3]. This paper describes the computer program DOCS (Design Optimization Codes for Structures), which represents an intermediate step in

achieving this objective of a general purpose design optimization software.

DOCS uses finite element analysis of the structure, well-developed design analysis methods and a simple optimization procedure. Main features of the code are: (1) Two and three dimensional structural systems can be modelled using rod and beam elements of variable cross sections, and constant strain triangular, shear panel and fiber reinforced composite finite elements, (2) large structural systems are handled by the use of substructural formulation, (3) damage-tolerant design capability is provided by including in the design process the probable future damage to the structure, (4) American Institute of Steel Construction and Aluminum Association of America specifications can be used in the design process, (5) acceleration loads can be specified for the structure, and (6) free format input for the program has been designed that closely matches the input form for the NASTRAN computer program. Other flexibilities have been incorporated into the code and include design variable linking, fixed design status for parts of the structure, direct input of substructural stiffness and mass properties, as well as specification of various constraint combinations such as stress, deflection, member buckling, natural frequency and member sizes. Definition of the design optimization problem for the program is kept quite general.

In this paper, the application of DOCS to a framed structure and a composite closed helicopter tail-boom structure with and without damage considerations is described. Data and results are presented in Tables 1 - 8 and Figures 1 - 3. The code has been dveloped on the IBM 370/158 machine. It has been recently converted to CDC, PRIME and VAX computers with minimal effort, partially because all READ/WRITE statements for the direct access files are written in a separate subroutine which makes the program portable.

The reliability of DOCS has been checked by solving serveral small scale design problems in addition to the examples presented in this paper [4]. For some small scale examples, the design sensitivity analysis has been checked using closed form solutions. The analysis part of the program has been tested by comparing solutions with the well-known analysis code SAP4.

A variety of design environments can be handled with DOCS. These features make the program suitable for design of practical structural systems. Several extensions of the code are possible, such as expansion of the finite element library (sensitivity analyses for plate bending elements are currently being added to the code) and treatment of dynamic loads and user options for selecting different optimization algorithms.

6

REFERENCES

1. Arora, J.S. and Haug, E.J., "Efficient Optimal Design of Structures by Generalized Steepest Descent Programming", Int. J. for Num. Meth. in Engrg., Vol. 10, No. 4, 1976, pp. 747-766; and Vol. 10, No. 6, 1976, pp. 1420-1427.

2. Khot, M.S., Berke, L., Venkayya, V.B. and Schrade, K., "Optimum Deisgn of Composite Wing Structures with Twist Constraint for Aeroeleastic Tailoring", Technical Report AFFDL - TR - 76 - 117. Air Force Flight Dynamics Laboratory. Wright-Patterson AFB, Ohio 45433.

3. Gallagher, R.H., et al., Optimum Structural Design, proceedings of the International Symposium, University of Arizona, Tucson, Arizona, Oct. 19-22, 1981.

4. Nguyen, D.T., Belegundu, A.D. and Arora, J.S., Sample Solutions with the Computer Program DOCS, Technical Report No. CAD-SS-82.9, Division of Materials Engineering The University of Iowa, Iowa City, IA, Feb. 1982.

TABLE I

SAMPLE INPUT DATA CARD FOR CROD ELEMENT·

Bulk Data Card CROD

Description: Specifies the properties of the truss element.

Format:

1	10 11	76	80
CROD	ℓ m_1 n_1 n_2 m_2		

Examples:

CROD   10   6   8   69   96

Remarks:

(i) ℓ: element identification number ($\ell > 0$)

m$_1$: materials property code number

n_1,n_2: grid points to which the element is connected

($n_1 \neq n_2$, $n_i > 0$)

m_2 : design variable code number (group number for members).

(ii) ℓ,n_i,m_j are all integer constants.

(iii) m_2 is unique unless design variable linking is implied.

TABLE II

DESIGN DATA FOR ONE-BAY, TWO-STORY FRAME

Modulus of Elasticity = 10900 ksi

Material weight density = 0.1 lb/in^3

Yield stress in tension/compression = 58 ksi

Yield stress in shear = 34 ksi

Lower limit on design variables = {1.0, 0.3, 0.1, 0.1} in
    (same for each group)

Cross-section used = I-section with four design variables

Upper limit on design variables = none

Displacement limits for 18 DOF: Limit on the ratio of the displacement of a joint to its height from the base is 0.002. Also, displacement limit within any element is $l_m/360$ where l_m is the length of the element. Thus, the limits are as follows:

Node	x_1 – limit (in)	x_2 – limit (in)
1	0.360	0.360
2	0.670	0.670
3	0.720	0.720
4	0.360	0.360
5	0.670	0.670
6	0.720	0.720

Number of loading cases = 2 (shown in Fig. 1)

Loading Condition Number	Load Description
I	45.0 kips along x_1 direction at Nodes 1, 3
II	0.5 k/in uniform loads along negative x_2 on elements 2, 3, 6, 7

9

TABLE III

RESULTS FOR ONE-BAY, TWO-STORY FRAME

Initial design (depth, flange width, web thickness and flange thickness):

$$b^{(0)} = \{(30.0, 15.0, 2.0, 2.0), (30.0, 15.0, 2.0, 2.0),$$
$$(30.0, 15.0, 2.0, 2.0), (30.0, 15.0, 2.0, 2.0)\} \quad \text{in.}$$

Initial Weight = 13.44 kips

Final design:

$$b = \{(30.142, 14.945, 0.6954, 1.7743), (30.1370, 14.9780, 1.0789, 1.8639)$$
$$(30.0210, 14.870, 0.3795, 1.0947), (30.0000, 14.892, 0.8436, 1.1752)\} \quad \text{in}$$

iteration	Weight (Kips)	Maximum Violation
1	13.440	0.0208
2	8.724	0.0720
3	8.088	0.0249
4	7.551	0.0026

Active Constraints at Optimum: Displacement limit along x_1 direction of Node 5 in loading condition 1.

Total CPU Time = 43.5 sec on IBM 370/158 in Double Precision.

TABLE IV

MATERIAL PROPERTIES AND ALLOWABLE STRENGTH OF BORON-EPOXY

Elastic modulus, E_{11}	30,000 ksi
Elastic modulus, E_{22}	27,000 ksi
Poisson's ratio	0.21
Shear modulus	6,500 ksi
Specific weight	0.0725 lbs/in^3
Allowable stress along fiber direction (tension)	176.0 ksi
Allowable stress along fiber direction (compression)	390.0 ksi
Allowable stress along transverse fiber direction (tension)	11.4 ksi
Allowable stress along transverse fiber direction (compression)	44.6 ksi
Allowable shear stress	2.1 ksi

TABLE V

DESIGN DATA FOR THE HELICOPTER TAIL-BOOM

Loading for the Structure

	Load Component (kips) in Direction		
Node Number	x	y	z
13	0.0	0.0	-0.140
14	0.0	0.0	-0.140
15	0.0	0.0	-0.140
16	0.0	0.0	-0.140
25	1.4903	1.6918	0.0
25	1.4903	-1.3658	0.0
27	-1.4903	1.6918	0.0
28	-1.4903	-1.3658	0.0

Lower bound on natural frequency = 29 Hz.

Data for Truss elements

Material: 2024-T3 aluminum alloy
Modulus of elasticity = 10,500 ksi
Stress limits = ±25.0 ksi

Material density = 0.1 lb/in3
Moment of inertia: $I = \beta A$; $\beta = 1.0$
Displacement limits = ± 0.50 in.
Lower limit on cross-sectional area = 0.0415 in^2
Upper limit on cross-sectional area = none

Data for skin elements (on two sides)

Material: 7075 - T6 Clad aluminum
Modulus of elasticity = 10,400 ksi
Stress limit = 40.2 ksi

Material density = 0.098 lb/in^3
Lower limit on thickness = 0.02 in
Upper limit on thickness = 0.50 in

TABLE VI

OPTIMUM DESIGNS FOR CLOSED HELICOPTER TAIL-BOOM
WITH COMPOSITE MATERIAL

Design Variable Number	Member Number	Example 3 (6 Damage Conditions)	Example 2 (No Damage)
1	2,3	0.17959D 00	0.41500D-01
2	1,4	0.29341D 00	0.41500D-01
3	5,6,9,10	0.24897D 00	0.41500D-01
4	7,8,11,12	0.14791D 00	0.48855D-01
5	13,15	0.41500D-01	0.41500D-01
6	14,16	0.41500D-01	0.41500D-01
7	17,18	0.21617D 00	0.41500D-01
8	20,21	0.84621D-01	0.41500D-01
9	19,22	0.13649D 00	0.41500D-01
10	23,24,27,28	0.11340D 00	0.41500D-01
11	25,26,29,30	0.16358D 00	0.48511D-01
12	31,33	0.41500D-01	0.41500D-01
13	32,34	0.41500D-01	0.41500D-01
14	35,36	0.63878D-01	0.41500D-01
15	38,39	0.46714D-01	0.41500D-01
16	37,40	0.55394D-01	0.41500D-01
17	41,42,45,46	0.41500D-01	0.41500D-01
18	43,44,47,48	0.48723D-01	0.50746D-01
19	49,51	0.41500D-01	0.41500D-01
20	50,52	0.41500D-01	0.41500D-01
21	53,54	0.61319D-01	0.41500D-01
22	56,57	0.41673D-01	0.41500D-01
23	55,58	0.44047D-01	0.41500D-01
24	59,60,63,64	0.41500D-01	0.41500D-01
25	61,62,65,66	0.63692D-01	0.41694D-01
26	67,69	0.41500D-01	0.41500D-01
27	68,70	0.41500D-01	0.41500D-01
28	71,72	0.54351D-01	0.41500D-01
29	74,75	0.53918D-01	0.41500D-01
30	73,76	0.72680D-01	0.41500D-01
31	77,78,81,82	0.18427D 00	0.41500D-01
32	79,80,83,84	0.17073D 00	0.44785D-01
33	85,87	0.41500D-01	0.41500D-01
34	86,88	0.41500D-01	0.41500D-01
35	89,90	0.87936D-01	0.41500D-01
36	92,93	0.41500D-01	0.41500D-01
37	91,94	0.41500D-01	0.41500D-01
38	95,96,99,100	0.41500D-01	0.41500D-01
39	97,98,101,102	0.70261D-01	0.41500D-01
40	103,105	0.41594D-01	0.41500D-01

13

TABLE VI (Continued)

Design Variable Number	Member Number	Example 3 (6 Damage Conditions)	Example 2 (No Damage)
41	104,106	0.41500D-01	0.41500D-01
42	107,108	0.19239D 00	0.50965D-01
43	1,2,3,4	0.67000D-02	0.11076D-01
44	1,2,3,4	0.67000D-02	0.67000D-02
45	1,2,3,4	0.92961D-02	0.16028D-01
46	5,6,7,8	0.86139D-02	0.72838D-02
47	5,6,7,8	0.16479D-01	0.11069D-01
48	5,6,7,8	0.67000D-02	0.67000D-02
49	9,10,11,12 13,14,15,16	0.67000D-02	0.82097D-02
50	9,10,11,12 13,14,15,16	0.67000D-02	0.82097D-02
51	9,10,11,12, 13,14,15,16	0.67000D-02	0.82097D-02
52	17,18,19,20	0.94398D-02	0.67000D-02
53	17,18,19,20	0.67000D-02	0.67000D-02
54	17,18,19,20	0.29438D-01	0.92058D-02
55	21,22,23,24	0.67000D-02	0.68632D-02
56	21,22,23,24	0.12386D-01	0.15024D-01
57	21,22,23,24	0.67000D-02	0.67000D-02
58	25,26,27,28, 29,30,31,32	0.12349D-01	0.97540D-02
59	25,26,27,28, 29,30,31,32	0.12349D-01	0.97540D-02
60	25,26,27,28, 29,30,31,32	0.12349D-01	0.97540D-02
61	33,34,35,36	0.67000D-02	0.67000D-02
62	33,34,35,36	0.85875D-02	0.67000D-02
63	33,34,35,36	0.16374D-01	0.90408D-02
64	37,38,39,40	0.12710D-01	0.67000D-02
65	37,38,39,40	0.14739D-01	0.69886D-02
66	37,38,39,40	0.67000D-02	0.67000D-02
67	41,42,43,44, 45,46,47,48	0.12710D-01	0.80420D-02
68	41,42,43,44, 45,46,47,48	0.12710D-01	0.80420D-02
69	41,42,43,44, 45,46,47,48	0.12710D-01	0.80420D-02

Structural Weight, lbs		61.50	40.34
CPU/Cycle, Sec IBM370-158		42.11	9.77

14

TABLE VII

CRITICAL CONSTRAINTS AT OPTIMUM FOR CLOSED TAIL-BOOM
WITH COMPOSITE MATERIAL

(a) Without Any Damage Conditions:

Stress constraint for members: 30,12,66,48,84

Lower bound on design variables: 8-10,12-14,1-3,5-7
44,48
22-24,26-28,15-17,19-21
52,53,57
36-41,29-31,33-35
61,62,64,66

(b) With 6 Damage Conditions:

Stress constraint for members: 27,36   Under damage condition: 1
48   2
66   3
102   4
71   5

Displacement in the y direction of node: 25   under damage
condition: 2,6

Lower bound on design variables: 12,13,5,6
43,44,48-51
24,26,27,17,19,20
53,55,57
36-38,41,33,34
61,66

TABLE VIII

(a) DAMAGE CONDITION DEFINITIONS FOR TRUSS MEMBERS

Truss Members

Damage Condition	Member(s) Damaged	Node(s) Damaged	%Reduction in Area
1	21,25,28,32,33, 35,39,44,45	10	100
2	1,6,12,13,16, 17,19,23,29	7	100
3	58,63,65,69,70 72,76,82,84	20	100
4	73,78,84,85,88 89,91,95,101	23	100
5	56,59,62,67,68 72,74,78,79	17	100
6	3.7.10,14,15, 17,21,26,27	6	100

(b) DAMAGE CONDITION DEFINITIONS FOR SKIN ELEMENTS

Skin Elements

Damage Condition	Member(s) Damaged	Node(s) Damaged	%Reduction in Area
1	7,8,11,12,21, 25	10	100
2	1,2,3,13,14,15	7	100
3	23,32,37,38,45,56	20	100
4	33-35,45-47	23	100
5	20,28,33,34,41,42	17	100
6	5-7,9-11	6	100

16
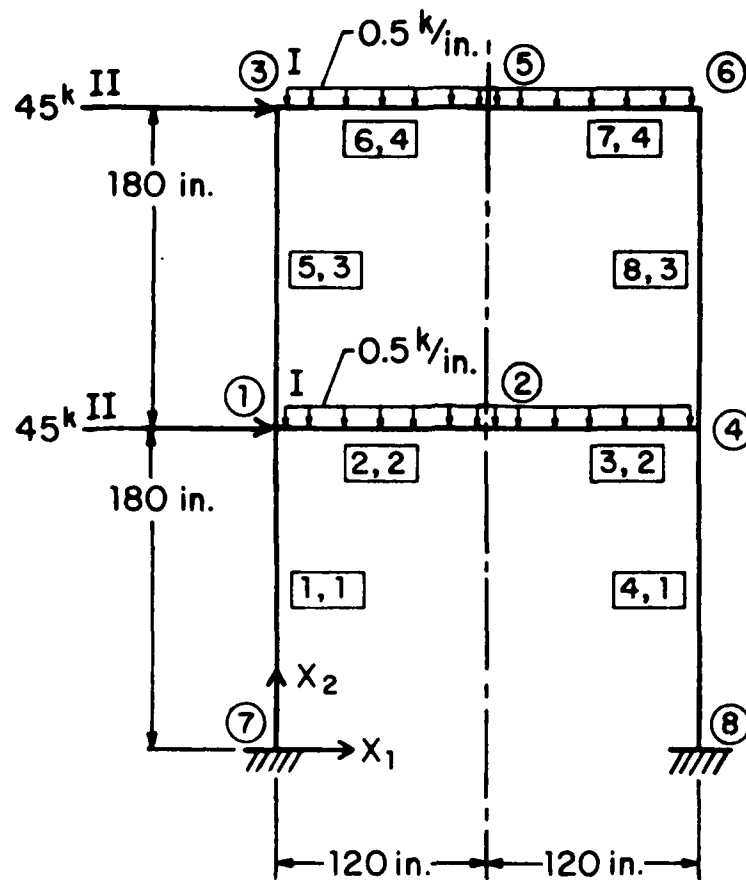
Figure 1: One-Bay, Two-Story Frame
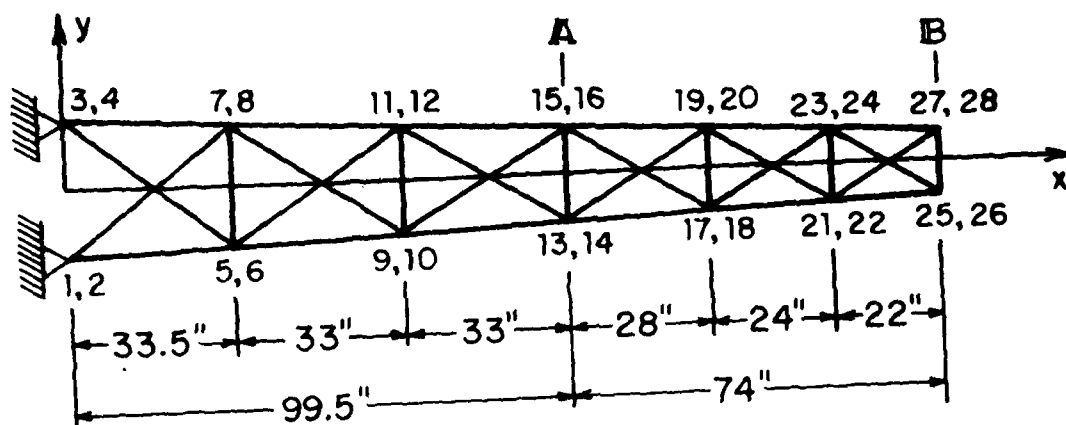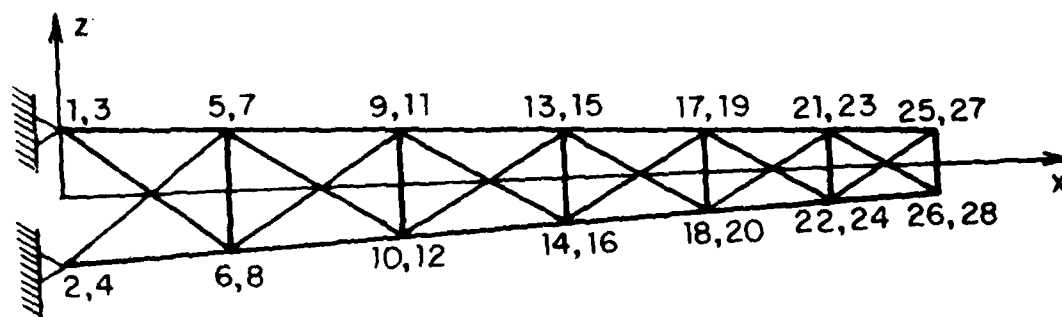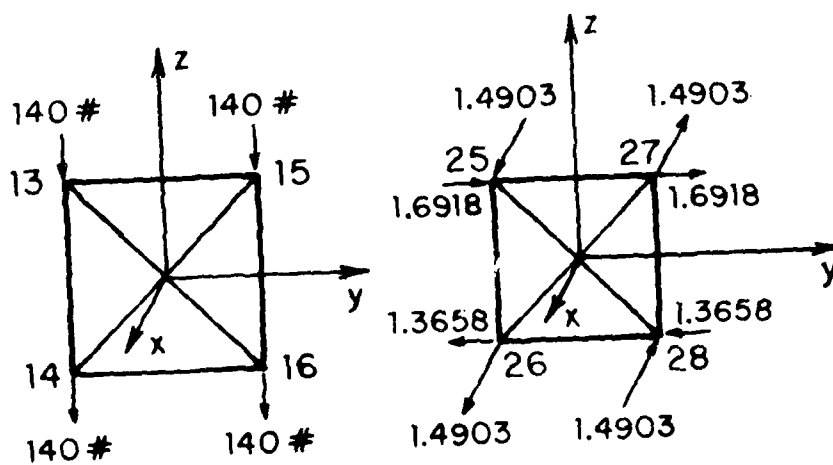
Figure 2: Arrangement of Members for the Helicopter Tail-Boom

18
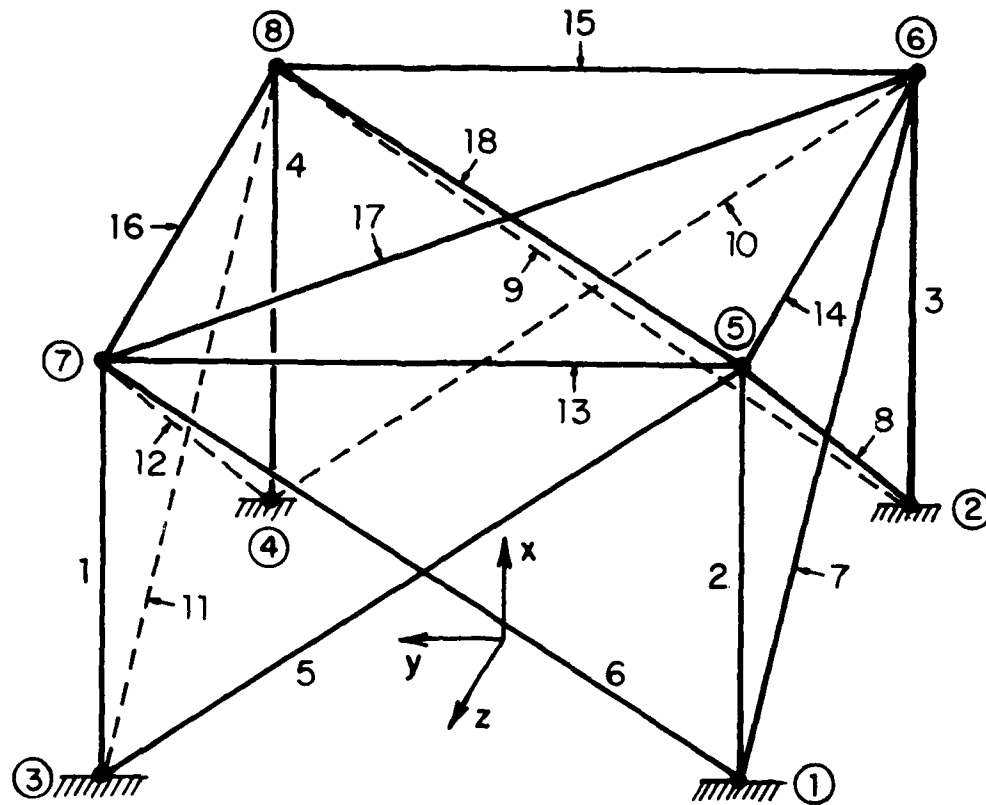
Following grouping of members, with members of a group to have same cross-sectional areas is used:

Group No.	Member Numbers
1	2, 3
2	1, 4
3	5, 6, 9, 10
4	7, 8, 11, 12
5	13, 15
6	14, 16
7	17, 18

Figure 3:- Truss Member Numbering for the First Panel

19

MEASUREMENT OF CRACK GROWTH IN ADHESIVE BONDS USING OPTICAL
INTERFERENCE FRINGE CONTOURS OF SURFACE DISPLACEMENTS

R. ANASTASI
Physicist
Army Materials and Mechanics Research Center
Watertown, MA 02172

J. ADACHI
Research Team Leader
Army Materials and Mechanics Research Center
Watertown, MA 02172

F. P. CHIANG
Moire Stress, Inc.
Port Jefferson, NY

ABSTRACT

A. INTRODUCTION

Deficiencies in the adhesive bond quality of a rotating-band-to-titanium-projectile diffusion bonded joint caused unpredictable rotating band failure, Figure 1, which recently jeopardized the time schedule of the projectile development program. Very apparent was the need for a systematic rational mechanics based method of evaluating adhesive bond quality that could be used for defining numerical bond strength requirements and for selecting, optimizing and controlling process and process variables.

The operating environment of a rotating band bond is extremely complicated involving radial compression, high shearing forces and possibly radial tension during the initial engraving process, high circumferential shear during projectile acceleration, and high radial tension stresses due to centrifugal forces after bond exit. Bond failures could easily occur under any one or combination of this sequence of forces resulting possibly in insufficient rotational velocity or the throwing off of the band when the projectile emerges from the confines of the gun tube. Stress analysis investigations and rotating band behavior studies under all these conditions are indispensable parts of the overall study but are not discussed in detail here. Of primary concern in this part of the study is the problem of measuring fracture properties of an adhesive bond system which when combined with the computed values of stress on the bond will determine whether or not the bond will fail.

A fracture mechanics concept forms the basis for the study and is due to Williams [1] as further developed by Bennett, Devries, and Williams [2]. A prerequisite for the use of this concept is the ability to measure the incremental growth of a disbonded area or "crack" in the adhesive bond interface. This can be done easily when the bonded materials are transparent and the "crack" outline can be seen directly. The two key steps of this study deal with the development of a method for measuring crack size in opaque materials

20

easily and accurately. They are the use of optical interferometry methods to
measure the deformation of the surface of the layer covering the disbonded
region and the relating of the shape and extent of the surface deformation to
the shape and extent of the subsurface crack.

B. ADHESIVE FRACTURES MECHANICS

Williams concept applies the principles of fracture mechanics to predict
adhesive fracture. A specific adhesive fracture energy, γ , is defined as the
energy released per unit of new surface created by the separation of adhered
dissimilar materials. The general equation based on a Griffith energy balance
analysis

$$\sigma_{cr} = K\sqrt{E\gamma/a}$$

can be applied for either cohesive or adhesive crack instability. Here σ_{cr} is
the applied stress at incipient failure, E is the elastic modulus, a is crack
dimension, K is a function of geometry and loading, and γ is the adhesive
fracture energy which characterizes the adhesive bond system and is dependent
on surface preparation, process condition process by products and any other
factor that may affect the character of the bond.

The test geometry considered here is the blister geometry shown in Fig. 2
consisting of a plate bonded to an essentially infinitely thick plate with a
hole through which pressure is introduced. As the pressure is increased, the
adhesive joint disbonds and a blister forms. A numerical analysis using a
finite element model as shown in Figure 3 examined the strain energy levels
corresponding to given pressures with incremental increases in disbond or crack
area and produced the nondimensional plot shown in Figure 4. In Figure 4
experimental data obtained from tests made with polyurethane (Solethon 113)
bonded to thick PMMA are shown superimposed on the analytical curve with excel-
lent agreement over a broad range of specimen geometry, h/a, indicating the
constancy of γ over the range of geometries. It is necessary merely to deter-
mine the values of p at which bond diameter a enlarges. Knowing the values of
E and h the value of γ can be directly determined.

C. DEBOND "CRACK" MEASUREMENT CONCEPT

The procedure described above requires the knowledge of the debond or
"crack diameter" corresponding to critical values of pressure, p. The proce-
dure being developed here involves the use of optical interferometry to measure
the contours of the deformation or "blister" of the visible upper surface of
the bonded plate.

A finite element analysis is being performed to determine the magnitude
and shape of the displacements of the visible upper surface for a range of
geometries to find if there exists a definite relationship between a definable
deformation "characteristic" of the upper surface (likely candidates are the
locations of maximum curvature or slope) and the location of the edge of the

21

debond that holds consistently over a range of geometry. With such a relation-ship it remains "only" to devise a technique that can easily detect and measure the deformation "characteristic." The making of this measurement is the key step in this study.

D. OPTICAL INTERFEROMETRY PROCEDURE

1. General

Two optical interferometric techniques have the potential for making the desired measurement of the deformation contour characteristic.

First order shadow Moire has the advantage of allowing continuous real time imaging of the deformation contours of a deforming surface as it deforms. However, its disadvantage is low sensitivity and trial tests have indicated that its sensitivity is too low for the magnitudes of deformation expected in the present tests.

Laser speckle interferometry requires a double exposure procedure rendering it unsuitable for real time imaging except by very expensive video storage, reconstruction and superpositioning processes. However, the procedure is very sensitive for measuring slope change and was selected for further investigation for this study.

2. Laser Speckle Interferometry for Slope Change Detection and Measurement

The main emphasis at this point is adapting laser speckle interferometry to measure blister (debond) radius. The basic optical arrangement of laser speckle interferometry is a laser illuminating an optically rough surface and a camera recording the laser speckle pattern at the surface. The method of Chiang [3] modifies this arrangement by focusing the camera on a plane a dis-tance A from the surface thus recording the speckles on this plane and not on the specimen surface Fig. 5. The speckle distributions on planes away from the specimen surface are very sensitive to surface tilting. When speckle distribu-tions before and after the surface undergoes out of plane bending, are super-imposed by double exposure, speckle redistributions caused by surface tilting cause speckle pattern interference.

These surface tilts are seen as fringes (partial slope contours) when the double exposure photograph is optically Fourier filtered (See Fig. 6). Fringes for tilt along any direction can be displayed by controlling the orientation of the filtering aperture in the transform plane. With the aperture placed at distance U_x or U_y from the origin along the X and Y axes respectively the fol-lowing relation for surface slope, ϕ, holds.

$$\phi_x = \frac{n \lambda L}{2 A U_x} \qquad \phi_y = \frac{n \lambda L}{2 A U_y}$$

Where, n, is the fringe order number; λ, is wavelength and L, is the distance from specklegram to transform plane.

For a quick test of the laser speckle method for determining debond radius, a specimen was made with a known debond. This specimen consisted of thin plastic sheet bonded to an aluminum plate except for a central two inch square area. The surface was painted white and one inch guidelines were drawn for scaling. The recording camera was focused one inch (25.4mm) in front of specimen surface. A double exposure photograph (specklegram) was made using f/4 aperture and Agfa 10E75 glass plate film. The center of the unbonded region was displaced 0.001" out of plane between exposures to simulate blister deformation. Optical Fourier filtering was done with one filtering aperture located at different angles in the transform plane in order to observe the effect of orientation on blister deformation fringe patterns - see Fig. 7.

To obtain a fringe pattern over the entire outline of the unbonded region, the number of filtering apertures at the transform plane was increased from one aperture to two apertures 90° apart equi-distant from the optical axis and finally to a complete ring aperture which produced the outline shown in Fig. 8.

The fringe patterns in Fig. 7 represent slope contours for slope in the directions parallel to the position vector of the aperture from the optical axis. The fringe pattern shapes are consistent with expected deformation contours of a blister. The one inch square grid can be seen faintly on the photographs of Fig. 7.

Using this grid as a scale the total distance from edge to edge of the fringe pattern measures two inches which is the size of the unbonded area of the test model. Thus the slope changes of the unbonded portions display clear fringe patterns and the bonded portions which undergo no slope change produce no fringe. The transitions from bonded to unbonded conditions on this test model is very well defined. Since the actual debond growth may not be symmetrical, it will be necessary to determine the entire outline. This apparently can be done by using the computer ring aperture as in Fig. 8.

E. CONCLUSION

The findings to date have indicated that slope changes in unbonded portions of adhesively bonded loaded plates produce fringe patterns the extent of which provides an accurate indication of the extent of the subsurface disbond. Whether or not a test can be devised so that the deformation in actual bonded copper models can be equally well detected is the major objective of the further studies current ongoing.

REFERENCES

1. Williams, M. L., "Stress Singularities, Adhesion and Fracture", Proc. of fifth U.S. National Congress of Applied Mechanics, 1966, P. 451-464.

2. Bennett, S. J., Devries, K. L., and Williams, M. L., "Adhesive Fracture Mechanics", International Journal of Fracture, Vol 10, No. 1, March 1974.

3. Chiang, F. P., and Juang, R. M., "Laser Speckle Interferometry for Plate Bending Problems", Applied Optics, Vol. 15, No. 9, September 1976.

FIG. 1 - TITANIUM ROCKET MOTOR BODY WITH DIFFUSION
BONDED COPPER ROTATING BAND
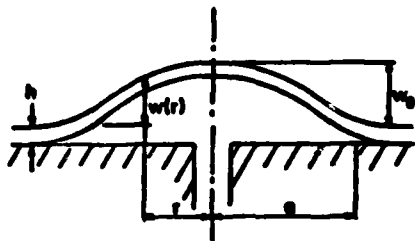
FIG. 2

SKETCH OF BONDED PLATE
GEOMETRY (FROM REFERENCE #2)

FIG. 3

DEBOND DEFORMED
GRID - THICK PLATE
(FROM REF. #2)

DEBOND DEFORMED GRID
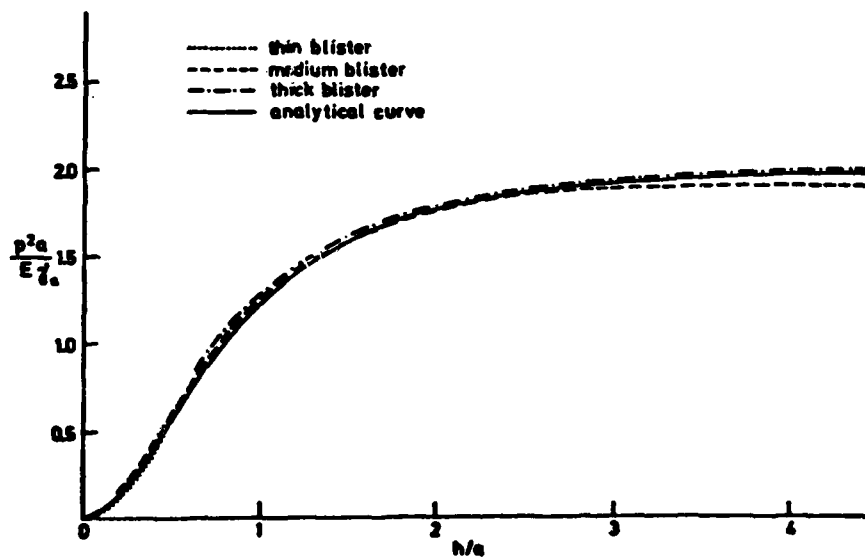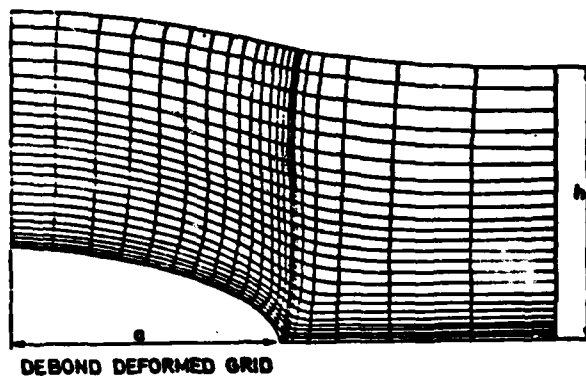
FIG. 4 - COMPARISON OF EXPERIMENTAL DATA AND
ANALYTICAL CURVE (FROM REFERENCE #2)

25
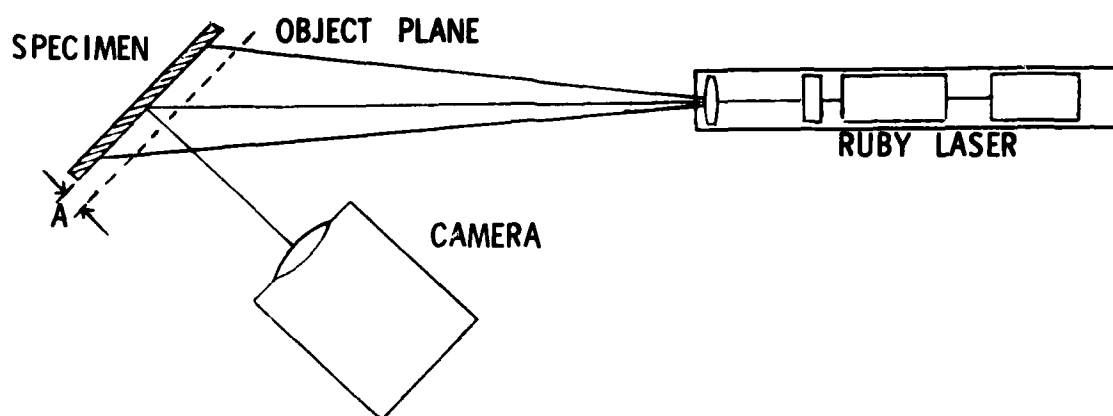
FIG. 5 - ARRANGEMENT FOR RECORDING LASER SPECKLES
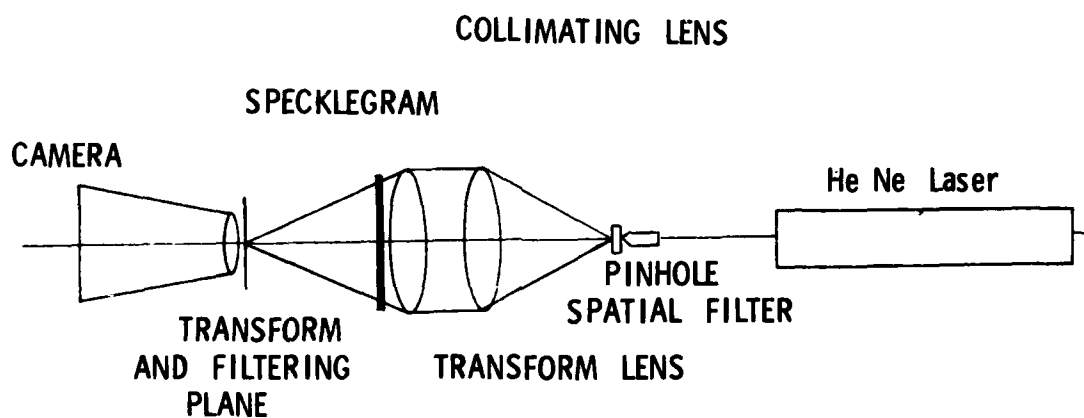
FIG. 6 - ARRANGEMENT FOR OPTICAL FOURIER FILTERING
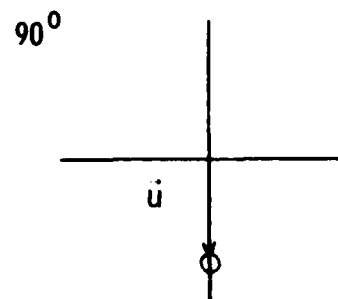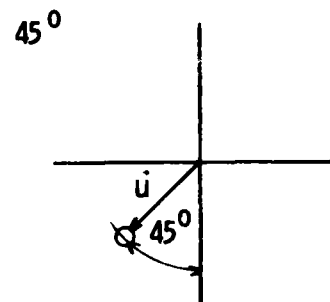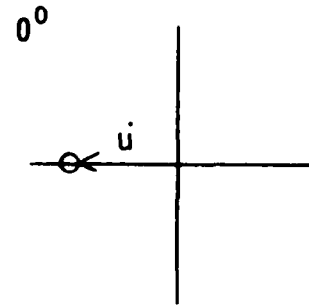
FIG. 7 - SLOPE CONTOURS, OBTAINED BY PLACING FILTERING APERTURE AT DIFFERENT ANGLES AT THE TRANSFORM PLANE u = 0.31 INCHES (7.8 mm)
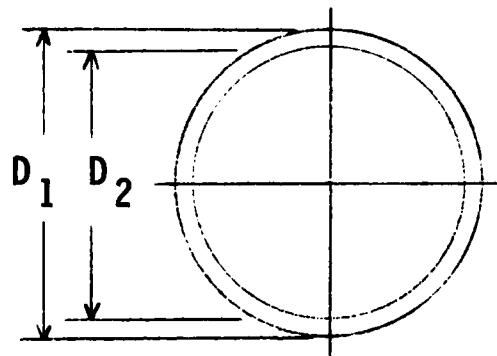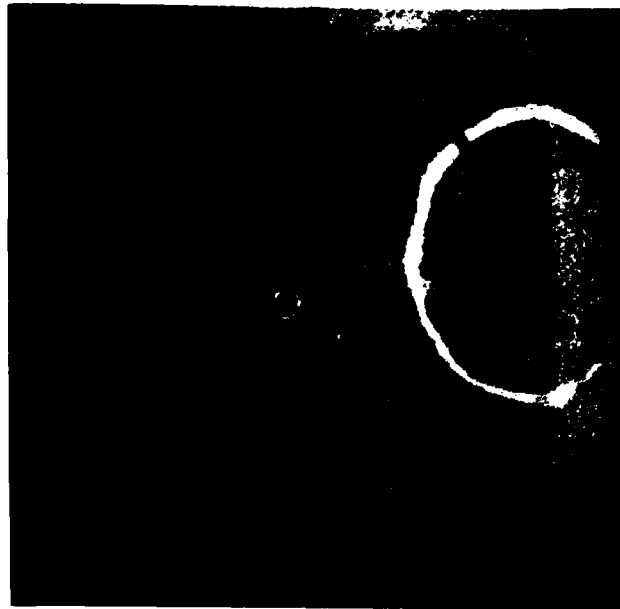
FIG. 8 - OUTLINE OF DEBOND, OBTAINED BY USING RING APERTURE
D_1 = 0.66 INCHES (16.7 mm) D_2 = 0.59 INCHES (14.9 mm)

IMPACT RESPONSE OF A CRACKED ORTHOTROPIC MEDIUM

M. K. KASSIR

Department of Civil Engineering

City College

City University of New York

New york, N.Y.   10031

ABSTRACT:

When a structural component is subjected to impact or shock loading, transient stress waves are generated, and the propagation of these waves can cause high stress elevation in local regions surrounding mechanical defects or cracks. In particular, near the vicinity of a crack tip, the magnitude of the dynamic stress-intensity factor is considerably larger than the corresponding statical one and in many instances may trigger crack extension and eventual failure of the member [1]. Thus, a knowledge of the overshoot in the dynamic stress-intensity factor and the time interval in which it occurs is essential to determine the response and fracture behavior of a structural member subjected to impact or shock loading.

The purpose of this study is to determine the elasto-dynamic response of an orthotropic solid containing a crack under the action of impact loading. An infinite orthotropic solid in plane stress(or plane strain) is assumed to contain a central *crack of length* (2a) in its mid-plane and subjected to a sudden state of loading. A system of cartesian coordinates (x, y, z) is chosen to coincide with the principal axes of elastic symmetry of the material and the crack is assumed to be situated in one of the coordinate planes(y = 0). Both normal impact loading as well as in-plane shear loading are considered, and the aim is to determine the distribution of the stress and displacement fields throughout the solid. In particular, attention is focused on finding out the degree of influence of material orthotropy on the amplification of the dynamic stress-intensity factor and on its duration.

Laplace and Fourier integral transforms are employed to reduce the two-dimensional wave propagation problem to the solution of a pair of dual integral equations in the Laplace transform plane. The solution of the dual equations is then reduced to the determination of an auxiliary function governed by a Fredholm integral equation of the second kind. Numerical methods are used to solve the Fredholm equation and to obtain the time dependence of the solution by way of a Laplace inversion

technique [2,3]. The dynamic stress-intensity factors for normal and in-plane shear loading, i.e. $k_1(t)$ and $k_2(t)$, are computed for several composites(listed in table below) and the normalized values are displayed graphically. For the composite materials considered, the overshoot in the value of $k_1(t)$ as compared to its statical value is about (16 - 18 %) and takes place in a time interval of ($C_s t/a$) = 2.2 - 2.6 seconds, while for mode 2, the amplification in the stress-intensity factor is about (4-8 %) and takes place in a time interval of ($C_s t/a$) = 2.0-2.5 seconds. Here, C_s stands for ρ / μ_{xy} with ρ being the mass density of the material.

The technique can be easily extended to treat edge crack problems and orthotropic materials with finite boundaries.

Table(I)   Elastic Constants

Material	E_x	E_y	μ_{xy}	ν
Boron-Epoxy type I	32.5×10^6psi (224.08GPa)	1.84×10^6psi (12.69GPa)	0.642×10^6psi (4.43GPa)	0.25
Boron-Epoxy type II	3.1×10^6psi (21.37GPa)	9.7×10^6psi (66.88GPa)	2.6×10^6psi (17.93GPa)	0.20
Glass-fiber (50%by volume)	5.55×10^6psi (38.27GPa)	1.33×10^6psi (9.17GPa)	0.54×10^6psi (3.72GPa)	0.28
Graphite-fiber (50% by volume)	25.2×10^6psi (173.75GPa)	1.0×10^6psi (6.89GPa)	0.55×10^6psi (3.79GPa)	0.28

REFERENCES:

1. Sih, G.C.(Editor), Elastodynamic Crack Problems, Mechanics of Fracture, vol.4, Noordhoff International Publishing, 1977
2. Krylov, V.I. and Kantorovich,L.V., Approximate Methods o꞉ Higher Analysis, Interscience, 1957.
3. Miller, M.K. and Guy, W,T., "Numerical Inversion of the Laplace Transform by use of Jacobi Polynomials", SIAM journal of numerical analysis, vol.3, 1966, pp.624-635.

ANALYSIS OF THE FREE EDGE PROBLEM IN COMPOSITES

O. L. BOWIE, C. E. FREESE AND D. M. TRACEY
Army Materials and Mechanics Research Center
Watertown, Massachusetts

ABSTRACT

The free edge problem of composite laminates has been treated by many
analysts using a variety of numerical formulations, yet there remain questions
as to exactly what the nature of the interlaminar stress gradient is near
the traction free edges. Some have concluded that there is a stress singularity
at certain interfaces in a cross-ply laminate, when the laminate is modeled
as a system of bonded orthotropic elastic sheets. Analytical work by Bogy
lends credence to this view, although his work is on the problem of bonded
isotropic materials. Other numerical analysts have concluded that while
there is a stress gradient across the interfaces, when the laminate is
being stretched, the free edge stress state is non-singular.

Whereas the laminate problem is generally three-dimensional in nature,
we have concentrated on the simpler planar elasticity composite problem, as
did Bogy. A representative problem is illustrated in Figure 1. The issue
there is the form of stress distribution along the interface between
materials 1 and 2. We have significant results to report in two areas, one
analytical, the other numerical. Analytically, we approached Bogy's asymptotic
problem, Figure 2, using the complex variable method. The power singularity,
which has stress varying as $r^{\lambda-1}$, $0<\lambda< 1$, found by Bogy for certain isotropic
composites, was verified for the isotropic case, but importantly, the
orthotropic solution was also obtained. Numerically, we developed techniques
for treating problems such as shown in Figure 1 using the finite element
method, accounting when necessary for the free surface singularity.

In isotropic complex variable elasticity, the solution is represented
by the analytic stress functions $\phi(x+iy)$ and $\Psi(x+iy)$. Although Bogy approached
the problem using the Mellin transform technique, his results suggest that ϕ
and Ψ can take the form $(x+iy)^{\lambda}$ near the interface-boundary intersection.
We chose this form in our analysis and verified Bogy's relationship between λ
and the properties of the two materials, by invoking the interface continuity
and traction free boundary conditions. We were able to go further than Bogy
and found the "eigensolution", i.e. the form of the stress solution around

the intersection. A similar analysis of the orthotropic case was conducted. Singular forms were chosen for the pertinent analytic functions of $x+s_1 y$ and $x+s_2 y$, where s_1 and s_2 are the material dependent roots defined in Leknitskii's formulation. As for the isotropic case, a complete solution to the eigen-problem was obtained.

The asymptotic results show that the r^λ singularity applies only to certain material combinations and not to others. It can be assumed that the same holds true for the 3D laminate problem, and thus it is not surprising that conflicting conclusions have been drawn concerning the nature of the free edge stress gradient. Of course, there is the fundamental deficiency of standard numerical methods to accurately model the behavior near a singularity that also contributes to the confusion.

We implemented a singularity finite element formulation to treat planar problems. The asymptotic solution sets the value of λ and this defines the particular singularity element displacement interpolation function. An isotropic problem that was considered is illustrated in Figure 3. The materials have shear moduli differing by a factor of 10 and for this plane strain case λ equals 0.8014. In this trial analysis a very fine mesh was used. The substructure including the intersection point is drawn separate from the main mesh. The polar grid is used to represent the angular gradients. The triangular elements at the end of the interface are given the singular interpolation function. The issues in this analysis have to do with the region of influence of the singularity and the magnitude of the stress amplication associated with the singular field. Results for the stress variation along the bondline are given in Figure 4.

The discussion will include presentation of the mathematical basis of our work. Comparisons between the numerical results and the asymptotic predictions will be presented. Finally, the considerations for extending the work to the important 3D laminate problem will be discussed.

FIGURE 1

FIGURE 2

FIGURE 3

34
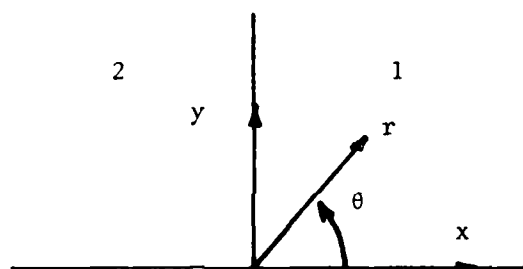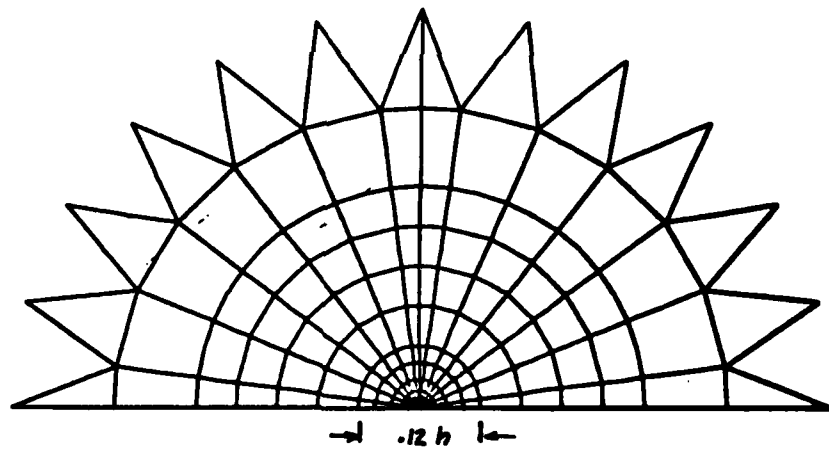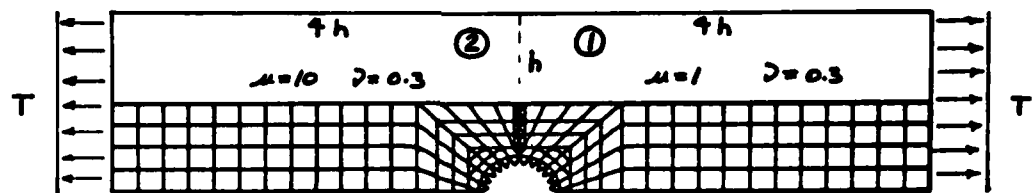
STRESS VARIATION ALONG BONDLINE
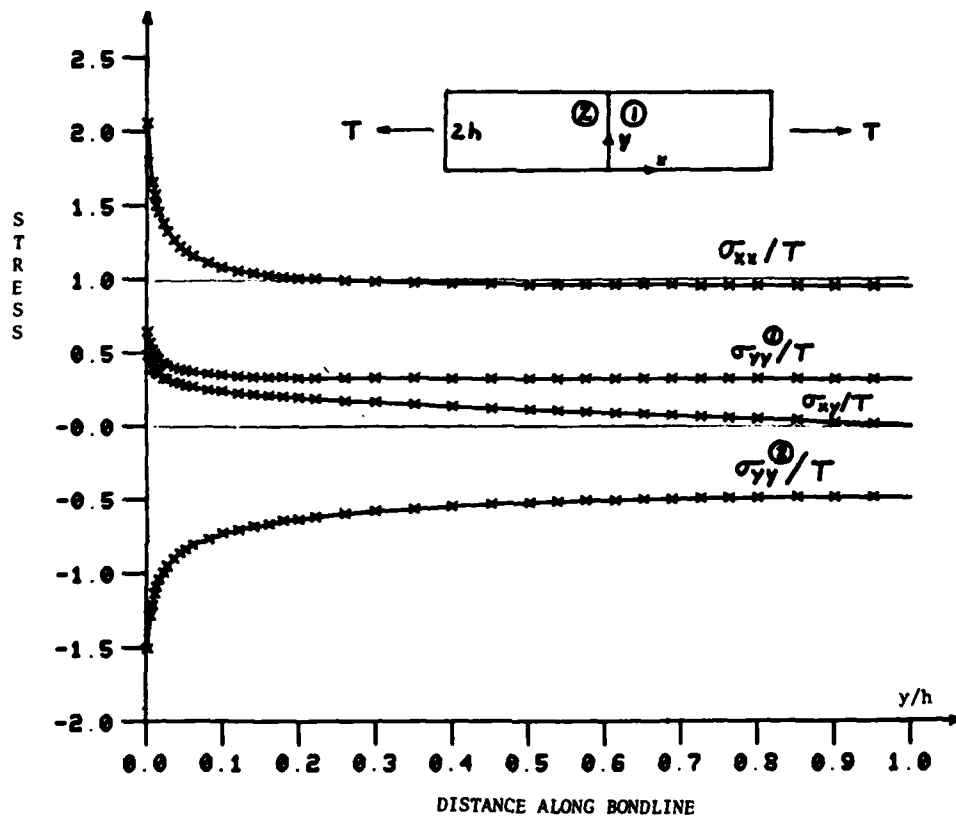
FIGURE 4

AN INVESTIGATION OF THREE-POINT AND FOUR-POINT BEND TESTS

JOSEPH R. PETERS
Mechanical Engineer
Army Materials and Mechanics Research Center
Watertown, MA 02172

ABSTRACT

When ceramic specimens are fractured utilizing three and four point bend tests, a microscopic examination is usually made of the fracture surface. However, many times the specimen is found fractured in many pieces, and it becomes difficult and time consuming to determine which fracture was caused by the loading stress.

High speed movies will be presented showing various ceramic materials fracturing in both three and four point bending. An attempt will be made to explore the movement of the fractured pieces at fracture and shortly afterwards. One of the questions to be addressed is, does the specimen receive multiple fractures because of physically striking the testing fixture, or are the fractures caused by shock waves, or both?

Future work will include very high speed photographs in an attempt to analyze the actual fracture. Some unexpected fracture sequences have been observed, and the qualitative behavior of loading fixtures is being evaluated.

THERMAL MECHANICAL FATIGUE SCREENING METHOD FOR GAS TURBINE ENGINE APPLICATIONS

J. R. WARREN
Engineering Specialist

B. A. COWLES
Assistant Materials Project Engineer
Pratt & Whitney Aircraft Group
Government Products Division
West Palm Beach, Florida 33402

EXTENDED ABSTRACT

BACKGROUND

Current and future military fighter aircraft require engines with rapid acceleration and deceleration capabilities for combat maneuverability. Coupled with requirements for engines with higher thrust-to-weight ratios, and correspondingly higher operating combustor exist temperatures, the severe turbine airfoil thermal fatigue environment has become and will continue to be the life-limiting degradation mode of turbine airfoils. Alloy and coating system evaluation and accurate service life predictions for advanced turbine blades and vanes are dependent upon realistic laboratory simulation of the engine service environment. For laboratory testing and analysis of material behavior, engine conditions are best simulated by mechanical testing capable of imposing simultaneous, independently controlled temperature and strain cycles, or thermal mechanical fatigue (TMF) tests. Historically, TMF tests have required expensive test specimens and sophisticated, usually computer controlled laboratory equipment. As a result, the cost of TMF testing has often been prohibitively expensive for airfoil material and coating system screening tests to optimize alloy selection. This has posed a continuing problem in gas turbine engine design in that less representative isothermal or thermal fatigue tests have been substituted and have formed the basis for material selections and life predictions.

OBJECTIVES

The objective of the current research is to develop and evaluate a flexible, low cost TMF test suitable for use in alloy/coating system research and screening tests.

DISCUSSION

In the gas turbine engine airfoil, thermal stresses arise from the differential thermal expansion between hot and cool locations on the component. During engine power transients (i.e. from idle to take-off power level), the more rapidly heated portions of the airfoil in the combustion gas path are placed in compression on heating. These same

locations see tensile stresses on cooling, and can be represented by an out-of-phase mechanical strain vs. temperature cycle as shown in Figure 1. These conditions are of primary concern in a coated system because tensile strain can approach or exceed the fracture strain of the coating at low temperature, thus promoting nucleation and propagation of fatigue cracks.

Since the engine airfoil environment is thermally driven, strain rather than stress is the independent mechanical variable and the optimum TMF testing technique is strain controlled. Unfortunately such testing is expensive because of the requirement for sophisticated equipment and instrumentation and large, precision-machined specimens. Since extensive fatigue data must usually be accumulated to establish statistical confidence and correlation with engine experience, the cost of the strain-controlled TMF test is a significant drawback.

To alleviate this problem, a "pseudo-strain controlled" or load adjusted TMF test was developed. In principle, the equipment and specimen design permit the same selection of thermal and mechanical parameters as in the strain controlled test, although the computed strain range is not as accurate as that directly measured by extensometry on large samples. However, the ability of the load adjusted test to generate consistent, interpretable data in good agreement with basic principles, engine experience, and the more sophisticated strain controlled testing technique has been demonstrated. The test equipment and test specimen are significantly less complex than that required to conduct a computer automated and controlled TMF test using the "strain control" test mode.

This method uses load rather than strain as the primary mechanical control parameter. Overall specimen gage axial displacement is measured and provides a coarse approximation of the sum of both mechanical and thermal cyclic strains. Since the thermal component of cyclic strain is essentially constant (from the fixed temperature endpoints of the temperature cycle) throughout the test, any deviation in cyclic displacement would be attributed to creep or strain hardening/softening and therefore would indicate a drift in the strain endpoints of the TMF test. If the displacement cycle is closely monitored and the load waveform stress endpoints are periodically adjusted to maintain constant displacement endpoints, a "psuedo-strain control" test can be achieved at approximately one-fourth the cost of a sophisticated computer-automated strain control TMF test. This mean stress shift in the load waveform is analogous to that which occurs on the computer strain controlled TMF test run at similar test conditions. In both tests the stress-strain hysteresis loops quickly stabilize and the tests then continue to failure at near constant load limits.

The test equipment is a conventional low cycle fatigue (LCF) test machine modified to simultaneously ramp and control temperature. The machine contains two electronically controlled servosystems: one is a hydraulic system for closed-loop control of load, strain, or displacement; the other servosystem is used concurrently for closed-loop control of specimen temperature. The temperature control system utilizes direct

resistance heating from a low voltage-high current transformer. A typical heated specimen is shown in Figure 2. For temperature measurement and control an infrared pyrometer is sighted on the specimen gage which allows high temperature TMF tests in the 500° to 2500°F range.

Test results for conventional blade/vane alloys using the "load-adjusted" TMF test method show good correlation (within a factor of two) with the full computer automated strain control TMF test results. (See Figure 3).

Other TMF tests using this method for screening, and coating development demonstrate that coatings have a great influence on fatigue life. Figure 4 shows the effect of coatings on TMF behavior and the fact that the coating generally results in a debit in fatigue life. The magnitude of the debit depends on the type of coating, its thermal expansion coefficient mismatch to the base alloy, and the strain range.

Work is currently in progress involving higher temperatures, hold times to include the effects of creep and oxidation, and more complex engine "mission" TMF test cycles for better engine environment simulation.

CONCLUSIONS

A low cost TMF test has been devised which can be used for simulating the thermal fatigue environment of high temperature components in aircraft gas turbine engines. The method is versatile and can be adapted to a wide range of test parameters (stress, strain, temperature, frequency) to aid in the design or screening development of advanced materials and coatings.
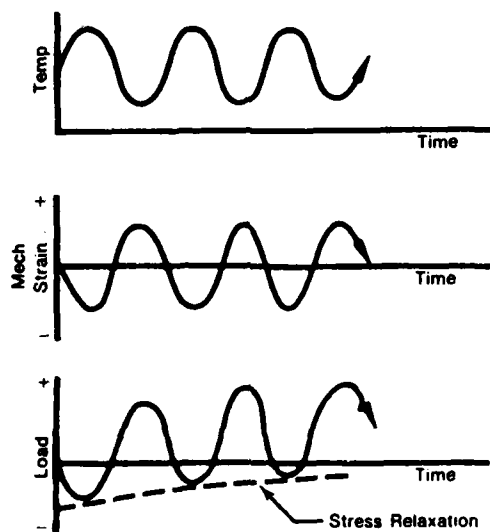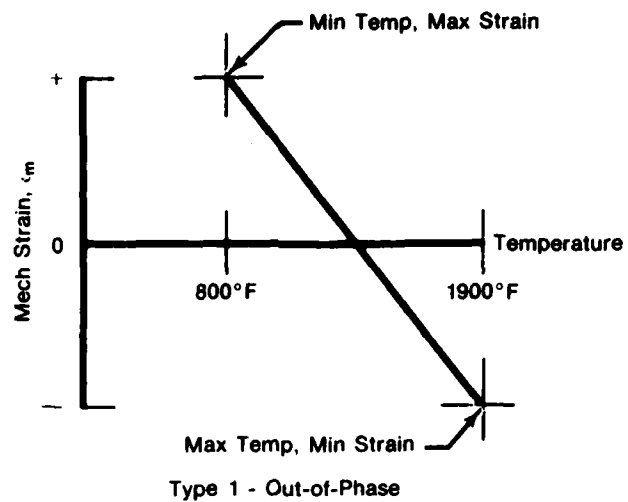
Figure 1.   Out-of-Phase TMF Test Cycle Mechanical Behavior
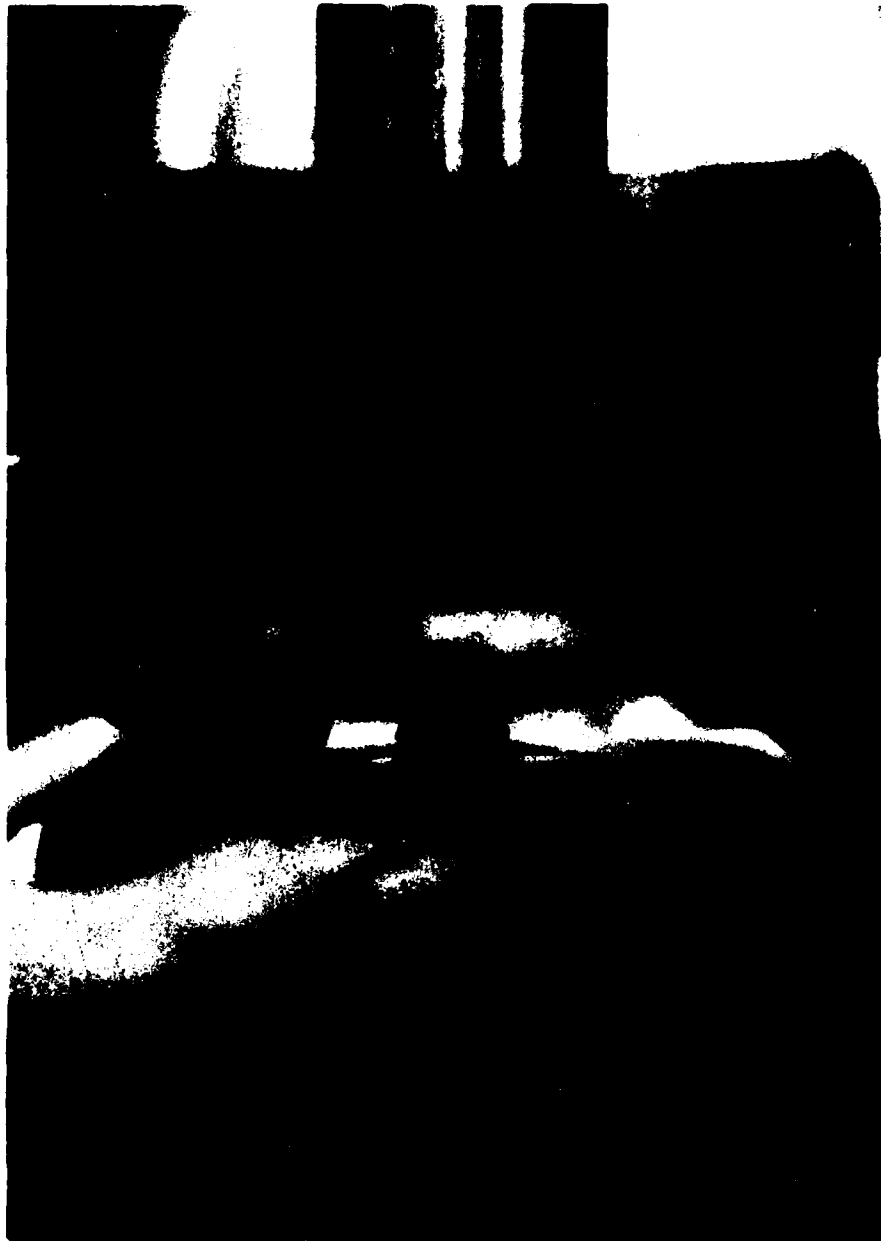
40

Figure 2.   Load Controlled TMF Test Specimen

41

Alloy: Coated MAR-M-200+Hf (Directionally Solidified)
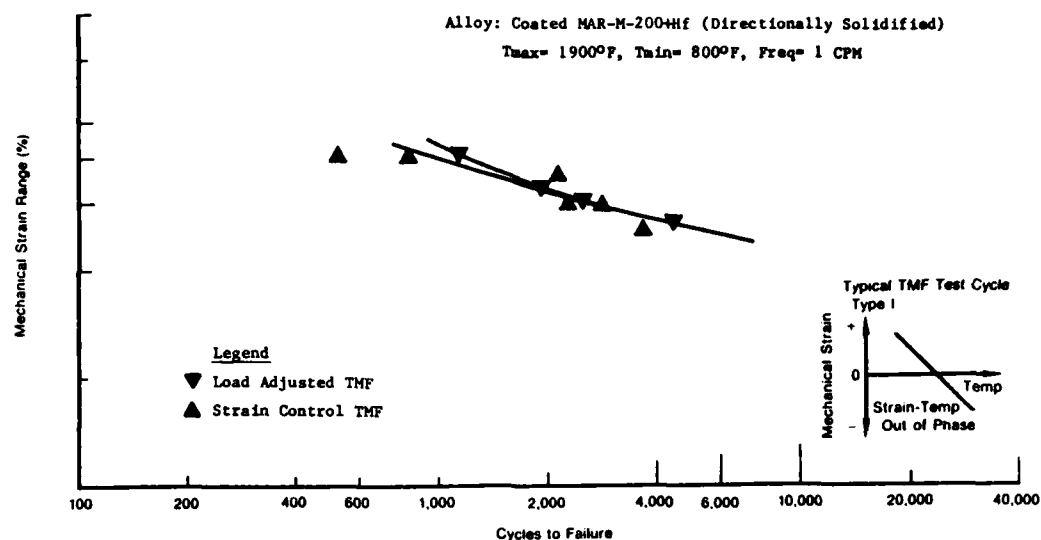Tmax= 1900°F, Tmin= 800°F, Freq= 1 CPM
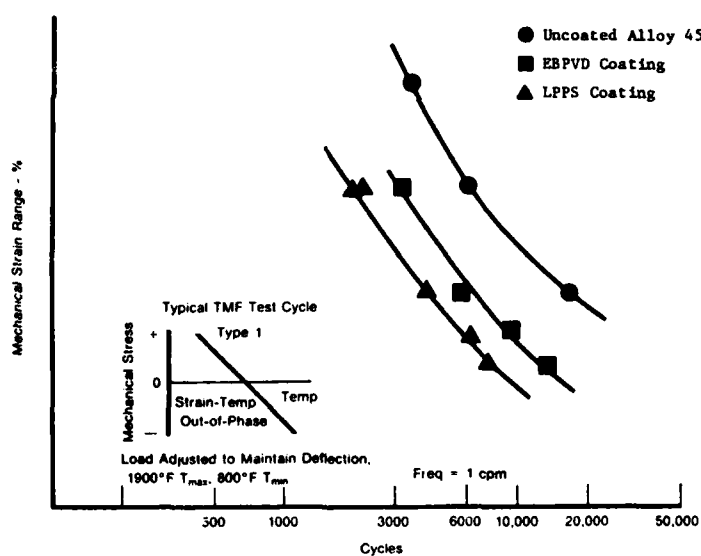
Figure 3.   TMF Test Method Comparison

Figure 4.   Effect of Coatings on TMF Life

42

EDDY CURRENT MEASUREMENT OF RESIDUAL STRESSES

W. G. Clark, Jr.
Materials Engineering Department
Westinghouse R&D Center

ABSTRACT

Accurate knowledge of the stresses and strains associated with the service loading of structural components is critical to the design of safe, efficient hardware. Common practice is to estimate expected loading conditions through the use of analytical methods and subsequently, to verify these estimates through strain-gage monitoring of models or actual operating equipment. This approach to stress analysis while often used successfully, has several limitations. Specifically, strains can only be measured at predetermined gage locations and strain gages alone cannot be used to detect residual stresses which may have developed during fabrication. This presentation describes an exploratory investigation conducted to evaluate the applicability of state-of-the-art eddy current nondestructive evaluation techniques to the characterization of applied and residual stresses in structural steels. Eddy current response (change in impedance) versus stress measurements were developed for ASTM Type A533B and A471 steels under tensile, bending and residual stress loading conditions. A "shrink fit" specimen was used to establish applicability to residual stress problems. Results show that an eddy current approach based on the use of commercially available equipment and a manual inspection technique can be used to provide an accurate quantitative measure of surface stresses. The technique can also be used to map surface stress contours. Details of the procedure are described along with the test results and proposed applications. Recommendations for further work needed to optimize and expand the technique are included.

DIFFUSION BONDED ROTATING BAND ON TITANIUM BASE PROJECTILE

JACOB GREENSPAN
Metallurgist
Army Materials and Mechanics Research Center
Watertown, Massachusetts 02172

EXTENDED ABSTRACT

INTRODUCTION

This work in progress is a sequel to previous work on the subject, described in AMMRC MS 80-5, pp 40-49, September 1980, the proceedings of a similar symposium. The system supported by this work is a 155 mm projectile (XM 785), comprised of a body of lightweight high performance titanium alloy, with a rotating band of conventional copper, and with design constraints which impose unusually severe stress carrying requirements at the interface. Therefore, an unusually secure attachment of the rotating band is required. For this the development of a diffusion bond was undertaken. In the early development such diffusion bonds exhibited marginal feasibility, as reported in the above reference. The ensuing development, however, has progressed to a point of acceptable feasibility, and utilization of such diffusion bonded rotating bands continues, as described in the following.

DESCRIPTION

Diffusion Bonding

The diffusion bond that joins the copper rotating band to the titanium alloy projectile body is obtained by hot isostatic pressing. This process employs an isostatic pressing medium of hot inert gas which acts effectively on the projectile configuration. In practice, the projectile body-rotating band assembly is sealed in a jacket impervious to the pressing medium, and subjected to a pressure-temperature-time cycle which obtains and maintains the proper interfacial contact, and temperature, for interatomic diffusion to take place. Properly carried out, the entire interfacial area becomes diffusion bonded.

In the early work, the copper rotating band was diffusion bonded directly to the titanium alloy projectile. For convenience this is called "Approach I" and this bond is called type "A-B" bond with "A" denoting the rotating band material, and "B" the projectile body material. Consequently the diffusion bond is comprised of AB alloy with composition variable across the interface.

An important characteristic of the "A-B" diffusion bond is the metastable, non-equilibrium structure of the A B alloy continuum across the diffusion bond. Intermetallic phases, characteristics of the stable, equilibrium state of the copper-titanium binary system, shown in Figure 1, do not appear in the microstructure of the "A-B" diffusion bond, as shown in Figure 2, and therefore such phases are not visibly generated by the above said hot isostatic pressing cycle. Detriment to the strength of the diffusion bond, as might be associated with the presence of such intermetallic phases, is not present in laboratory shear strength test, since levels of 40 ksi or greater are exhibited. In such tests, the failure mode is not on the diffusion bond, but in the copper.

44

However, in gun firing proof tests some rotating bands have become stripped, as reported on the above reference. Of 28 such bodies, 16 rotating bands remained intact, 8 became partially stripped, and 4 became totally stripped. Figure 3 typifies these results.

Approach I therefore has exhibited a certain lack of tolerance for error, for causes not specifically known, though an incipient presence of Cu-Ti intermetallic phases has been suspect. In ongoing development a niobium interlayer has been introduced to function as a buffer zone. A photomicrograph is shown in Figure 4. Both the Nb-Cu, and Nb-Ti binary systems, Figure 5, exhibit continuous solid solubility throughout the entire compositional range, and therefore should be effective in this respect. For convenience, this diffusion bond is called Type "A-X-B", where A and B are as before, and X is the niobium interlayer. The processing by which this bond is obtained is now called "Approach II", and described further in the following. The "A-X-B" diffusion bond consequently consists of a zone of AX alloy of variable composition, a zone of X, and a zone of XB alloy of variable composition across the interface. In laboratory shear test, as for the AB bond, the failure mode is not in the diffusion bond, but in the copper.

The type A-X-B diffusion bond has thus far been proven totally effective in gun firing proof tests. Of nearly fifty bodies so tested, none has exhibited stripping of the rotating band from the projectile body.

Projectile Body

The processing is now described further in terms of the qualification properties of the titanium alloy projectile body. In Approach I, the procedure has been to obtain such properties by a solutionize-quench-age approach, according to established procedure for the Ti-6-6-2 alloy hereby employed. In this case, the diffusion bonding cycle is carried out on the qualified body under conditions (1200°F for 1 to 2 hours), which do not result in loss of strength or toughness. Minimum qualification properties are 160 ksi yield strength, 170 ksi tensile strength, 10% tensile elongation, and 8 foot pounds V notch charpy at -40°F.

In Approach II, a temperature of 1500°F (816°C) is required to obtain the A-X-B diffusion bond. Since the projectile body thereby becomes overaged, with loss of properties, the process now incorporates a solutionize-quench-age procedure on the banded body, to obtain the body qualified.

REMARKS

The "A-X-B" diffusion bond now makes possible the continuing utilization of the diffusion bonded rotating band in the XM 785 projectile system.

From the academic point of view, it may be noted that Approach II differs from Approach I in two major ways, (1) the Nb buffer to the formation of Cu-Ti intermetallic phases, and (2) higher temperature processing. While Approach I has not yet been investigated with respect to the latter, such an investigation could clarify the role of the presence of the intermetallic structures in the diffusion bond.

ACKNOWLEDGEMENTS

46

Cu-Ti Copper-Titanium
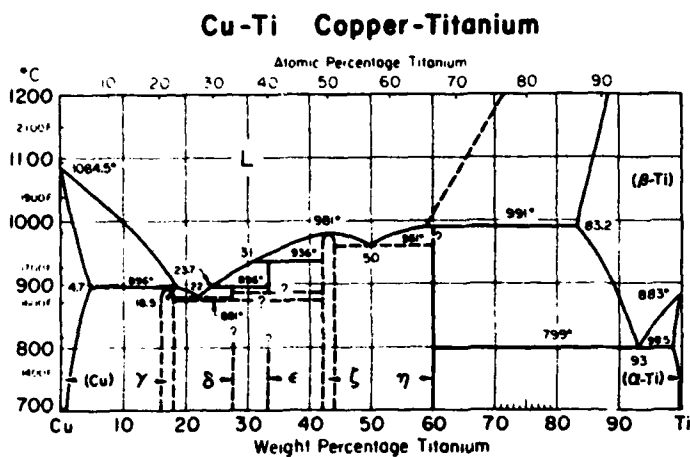
Figure 1. Copper-titanium binary system.

Ti-6-6-2   Cu ALLOY

Figure 2. Type "A-B" diffusion bond.

47

In launch - Band stripped

Recovered - Band partially stripped

Recovered - Band intact

Figure 3.

48

20 µ

Ti-6-6-2   Nb   Cu

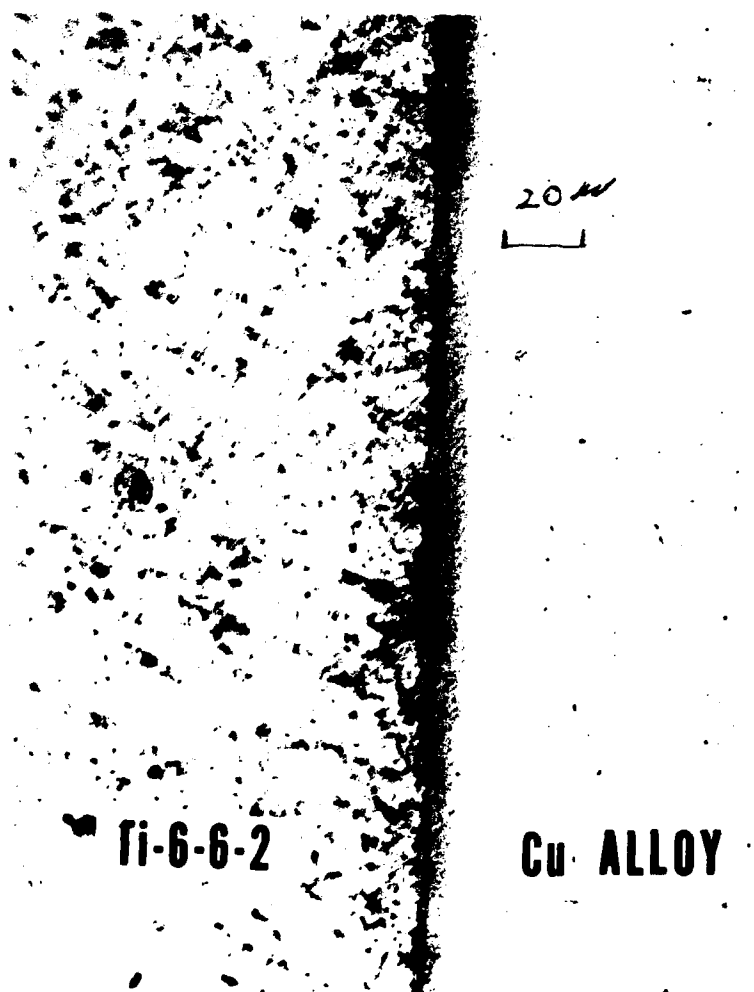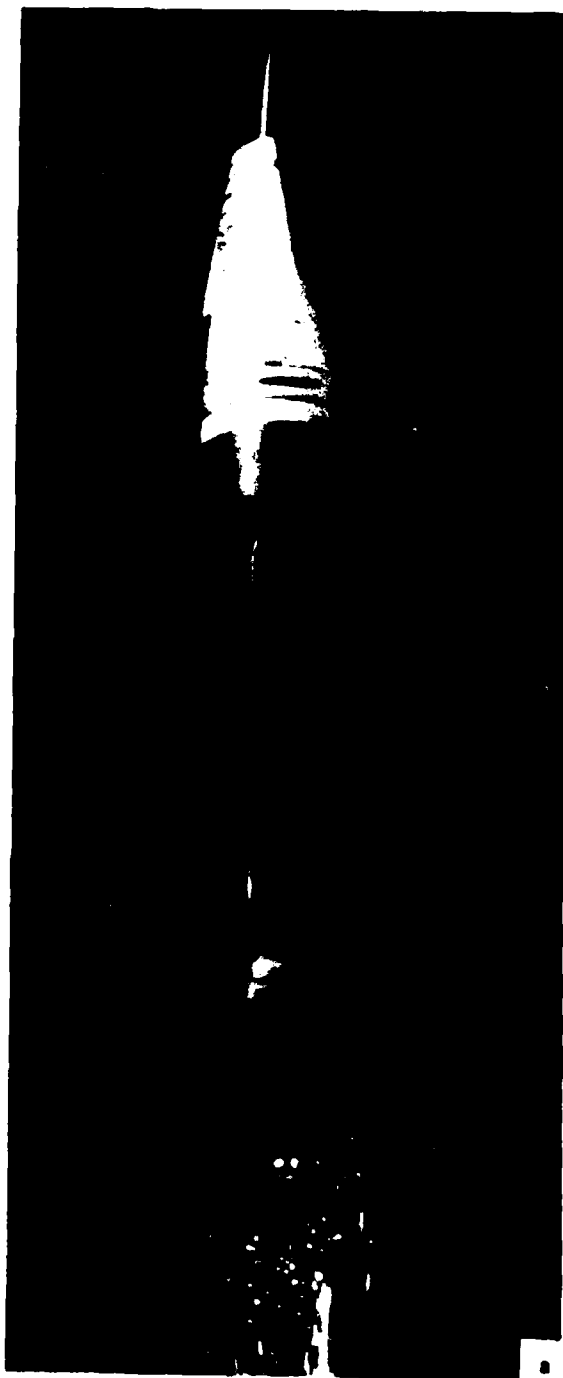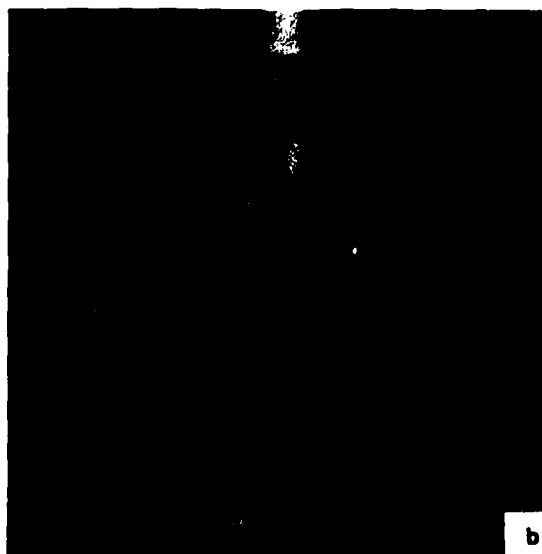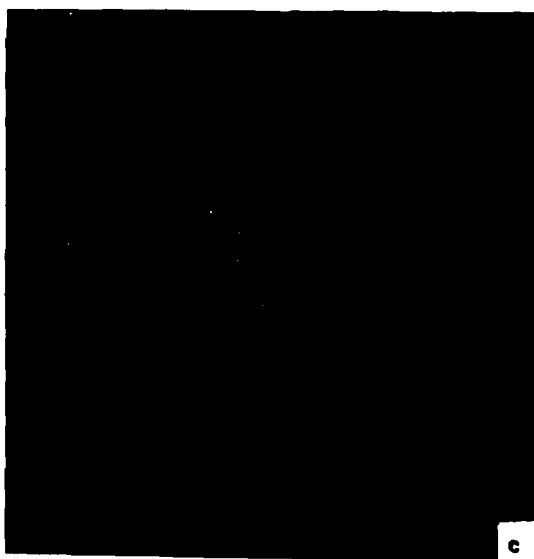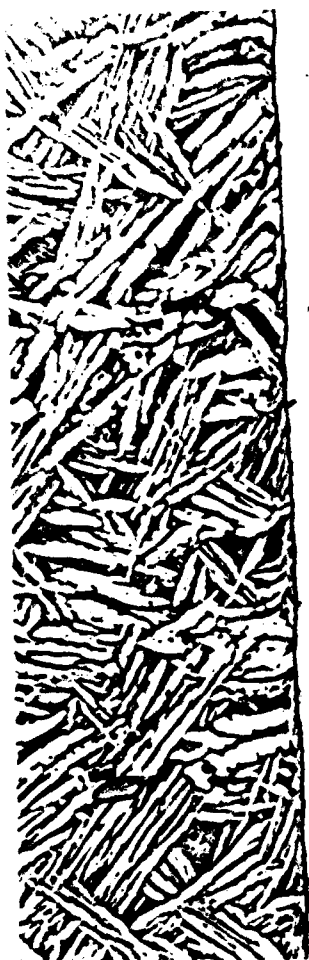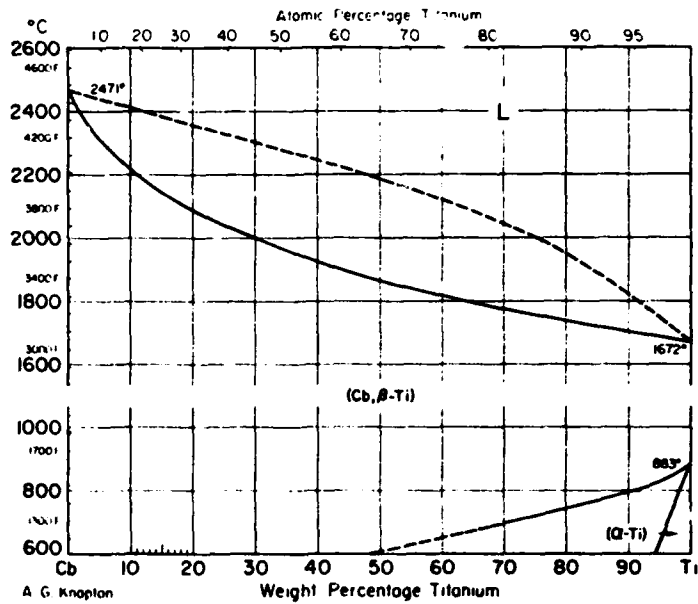Figure 4.   Type "A-X-B" diffusion bond.

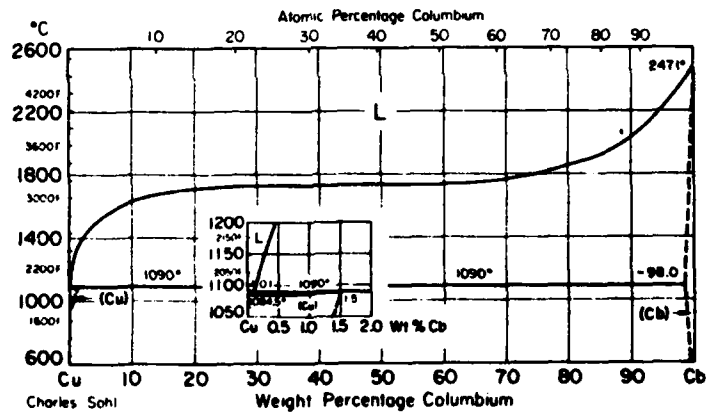## Nb-Ti Niobium-Titanium

Nb-Cu Niobium-Copper

Figure 5. Niobium-titanium binary system and niobium-copper binary system.

50

STRUCTURAL EVALUATION OF A DISCONTINUOUS SHELL
SUBJECTED TO AN INTERNAL BLAST

AARON DAS GUPTA
Mechanical Engineer

HENRY L. WISNIEWSKI
Mathematician
U S Army Ballistic Research Laboratory
Aberdeen Proving Ground, MD. 21005

EXTENDED ABSTRACT

Large deflection elastic-plastic response of a hemispherical contain-
ment shell configuration with an equipment access door opening supported on a
horizontal rigid foundation and subjected to an internal blast was analyzed
using a finite-difference structural response code, Petros 3.5, developed
at M.I.T.. The reflected overpressure loading was estimated from a scaled
distance of the wall from the point of detonation based on a conservative
cube-root scaling law and an exponential decay. The residual quasi-steady
load was obtained from an equation developed by Kinney and Sewell based on the
ratio of the available vent area and the internal volume.

Only a 180° segment of the structure was modeled using 22 meshpoints in
the circumferential and 39 meshpoints in the hoop direction except in the
cutout regions where only 31 meshpoints were used. Each mesh consists of four
Gaussian integration points through a single thickness layer. The constitu-
tive property of the material was approximated by three sublayers combined to
generate a trilinear strain hardening curve followed by a perfectly-plastic
behavior and a multilinear elastic-plastic unloading resulting in a polygonal
approximation.

The results indicate dynamic response behavior of the structure similar
to that of a continuous structure particularly at locations remote from the
pole and the wall opening area. However, for the discontinuous structure a
complex motion of the pole in the tangential direction in addition to radial
direction could be observed. Unlike the continuous structure where peak
stresses and strains occur at the clamped region near the base, high strains
were observed near the door opening area due to stress concentration at the
corners in the cutout. Peak resultant deflections occurred at the pole as
expected. Bending strain components dominated the response behavior near the
clamped region at the base and the cutout while the strains near the pole were
predominantly membrane strains. The resultant stresses and deflections were
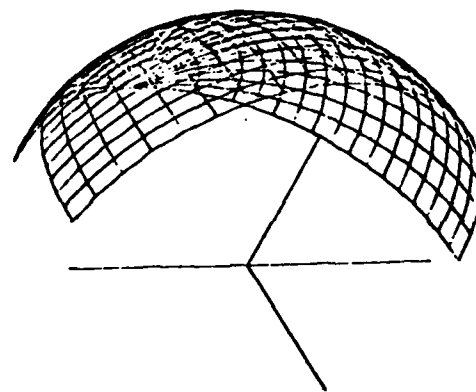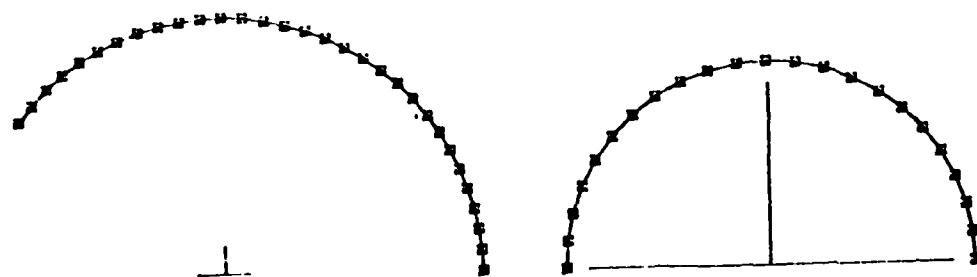in the elastic regime which satisfied the design requirements.

Figure 1 Initial configuration of the discontinuous hemispherical shell structure with access opening (scale: 1/2.0)

52
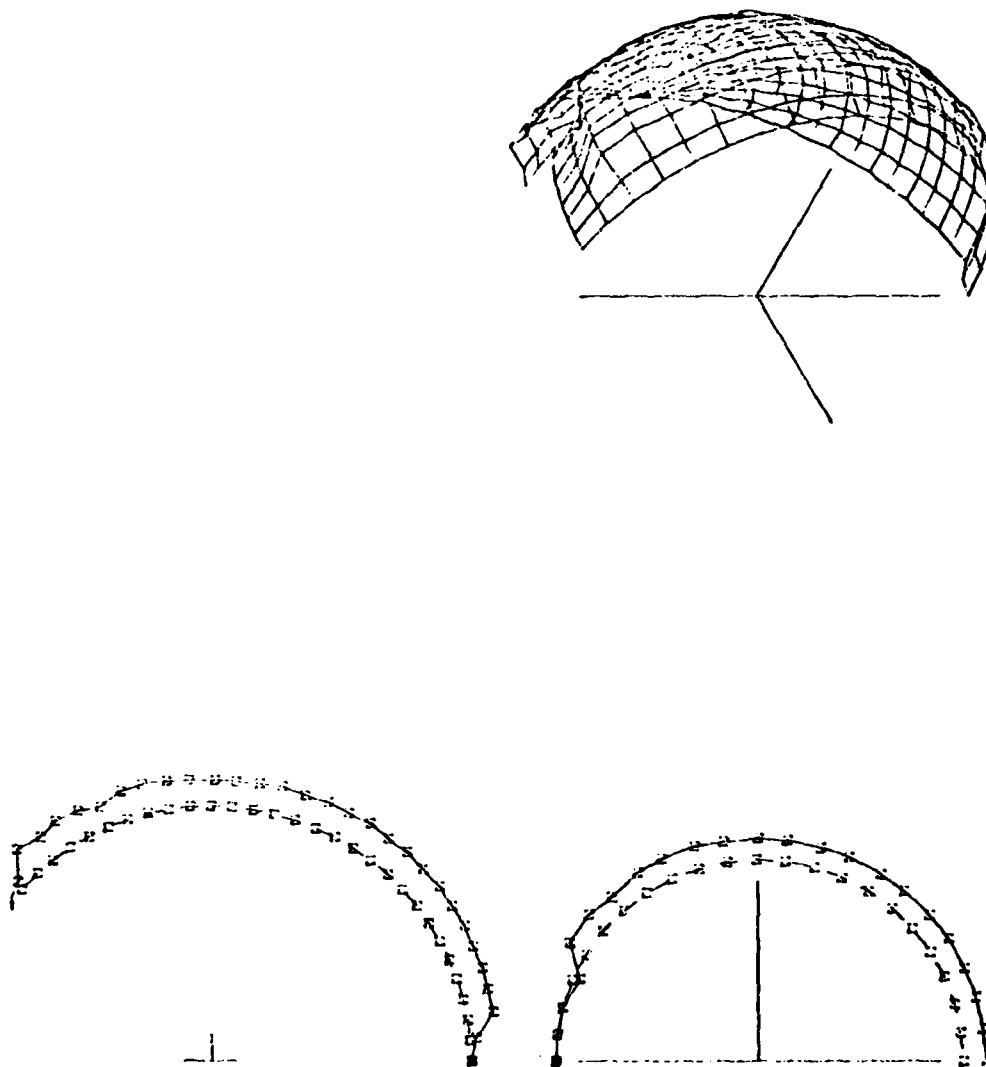
Figure 2 Deformed configuration of the discontinuous hemispherical shell structure due to an internal blast (deflection magnification: 1000)

53

THE ROLE OF NDE IN STRUCTURAL RISK ASSESSMENT

W. G. Clark, Jr.
Materials Engineering Department
Westinghouse R&D Center

ABSTRACT

Fracture mechanics concepts combined with probabilistic risk assessment techniques yield a unique methodology for the quantitative characterization of structural integrity. Such a "probabilistic fracture mechanics" approach to design permits a detailed evaluation of the effect and interaction of applied stress, material properties and inspection capabilities on the probability of failure. Armed with the appropriate statistical data, a probabilistic fracture mechanics analysis can provide the basis for a rational evaluation of design trade-offs so important in the risks-benefits approach to modern design decision making concepts.

A critical aspect of any probabilistic fracture mechanics analysis is the method used to address nondestructive inspection capabilities. Concern for the minimum defect size which can reliably be detected is important but other factors must be considered. For example, defect distribution, probability of flaw detection, inspection interval and the statistics of prior service experience can have a tremendous effect on the probability of failure.

In this presentation, a hypothetical problem is used to demonstrate the role of various nondestructive inspection considerations on the results of a probabilistic fracture mechanics risk assessment analysis. The structural integrity of a heavy section steel flywheel exposed to a service environment which can produce stress corrosion cracking is evaluated. The applied stress and material properties are held constant and the inspection concerns varied to reflect the influence of minimum detectable flaw size, probability of flaw detection, defect distribution and inspection interval on probability of failure. Results show that inspection considerations must be evaluated carefully to yield a rational risk assessment analysis.

THEME AREA: ADVANCED MATERIALS

Development of Low-Cost, Fine-Grained, Silicon Carbide Powder

by Cryogenic Milling

R.A.Penty, M.R.Wolman, W.S.Hubble, and I.G.Most
EnerGroup, Inc., 116 Commercial Street, Portland, Maine 04101

ABSTRACT

Cobalt, Chromium, nickel and niobium are imported from politically sensitive parts of the world. The use of silicon based ceramics to replace these materials would make the United States less dependent on potentially unstable foreign sources of raw materials.

This work involves developing a cryogenic milling process which can rapidly break down coarse crystals of silicon carbide made by the Acheson process to produce low-cost, fine-grained silicon carbide powder. This powder can be used to produce fully dense silicon carbide components by cold pressing and sintering to net shape.

An attritor mill was modified to operate at the temperature of liquid nitrogen. Cryogenic milling reduces the milling temperature and reduces any plastic deformation involved in the milling process resulting in a more brittle material which can be more easily reduced to a small particle size. Conventional room temperature milling was carried out as a comparison to milling in liquid nitrogen.

Powders cryogenically milled in the laboratory to an average particle size of approximately $1 \mu m$, as well as commercially available powders, were cold pressed and sintered at $2100°C$. The resulting samples were characterized with respect to:

(i)   density
(ii) three point modulus of rupture
(iii) microstructure by ceramographic techniques
(iv) fracture surfaces by scanning electron microscopy.

The cryogenic milling process will be described and the test results will be presented.

DYNAMIC CRACK PROPAGATION IN WELDED
STRUCTURES SUBJECTED TO EXPLOSIVE LOAD...G

M. F. KANNINEN
Research Leader

J. AHMAD
Principal Research Scientist

C. R. BARNES
Research Scientist

BATTELLE
Columbus, Ohio 43201

EXTENDED ABSTRACT

Welded regions very often are the most vulnerable areas in a
structure. Yet, applications of fracture mechanics to consider the
effect of defects in or around a weld have so far only been made in
simplistic ways. One reason is that accurate analyses of the weld-
induced residual stress and deformation fields that interact with the
crack growth process have not been available. Recently, however, it has
become possible to obtain reasonably accurate descriptions from finite
element simulations of the welding process. Coupling these with the
new fracture mechanics concepts that have evolved from concurrent progress
in crack growth initiation and propagation under elastic-plastic
conditions has made much more realistic analyses possible. The research
described in this work-in-progress summary addresses one aspect of this
general problem: dynamic crack propagation in a flawed structure in
which crack initiation occurs under an explosive loading.

BACKGROUND

With support from the Office of Naval Research, the authors have been
developing a fracture mechanics approach to cope with the complex conditions
appropriate for flawed ship structures under service conditions. This work
requires a three-fold generalization of the ordinary linear elastic fracture
mechanics (LEFM) techniques now in common use. Specifically, the approach
must accommodate: (1) the rapidly applied loads that could occur in an
attack situation, (2) the extensive crack tip plasticity that arises from
the high ductility and toughness of ship hull materials, and (3) the weld-
induced residual stress and deformation fields that accompany the flaws
that are present in a weld.

The objective of the research is to devise an analysis procedure that
is both reliable and practical. To meet the first of these requirements
the analysis must be fundamentally valid. To also be practical, because
of the likelihood of flaws occurring in complex structural conditions, the
procedure that is developed must be compatible with dynamic structural
analysis codes. To satisfy both requirements simultaneously, the fracture
properties required for the analysis must be obtainable from tests on simple
laboratory specimens.

APPROACH

The approach that has been taken in this research involves an integrated combination of fracture experiments and elastic-plastic finite element analyses. Attention has been focussed on the measurement and prediction of crack initiation, rapid propagation and arrest under quasi-static and dynamic loading conditions. In order to keep the effort manageable, a step-by-step procedure has been followed. Specifically, to initiate this work, attention was placed on monolithic high-strength components of a rate-insensitive model material (4340 steel), a simple specimen geometry (three-point-bend specimen) and a moderate rate loading condition (mechanical impact). Subsequent work has employed the ship structure steel HY-130 in a monolithic component and in an X-welded plate, both under explosive loading.

Work currently in progress involves blast loaded precracked plates of 4340 steel and (welded) HY-130. The loading fixture for the experiments is shown in Figure 1. Figure 2 shows two post-test specimens that were subjected to a 5-pound charge of C-4 explosive at a stand-off distance of 15 inches. It can clearly be seen that the 4340 steel plate was rapidly fractured while the welded HY-130 plate, while significantly deformed, remained intact. Approximately 0.25 inch of crack extension occurred in this experiment.

PRELIMINARY RESULTS AND EXPECTATIONS

The focal point of the current effort is a prediction of crack growth initiation, propagation and arrest under blast loading using the measured pressure history and basic material and fracture property data. To this end dynamic elastic-plastic finite element analyses are in progress using a critical value of the J parameter for initiation and a critical crack opening angle value for unstable crack propagation. (Crack arrest is viewed as the inability of the crack propagation process to continue.) The preliminary results suggest that reasonable results can be obtained provided the elastic-plastic deformation is accounted for; NB, elastodynamic treatments do not suffice. More detailed comparisons of the experiments and the analyses will be provided at the conference. Presuming that these are similarly encouraging, it can be anticipated that the ground work will have been provided for analyzing a range of problems beyond those encountered in ship structures; e.g., penetration/perforation events in armor.
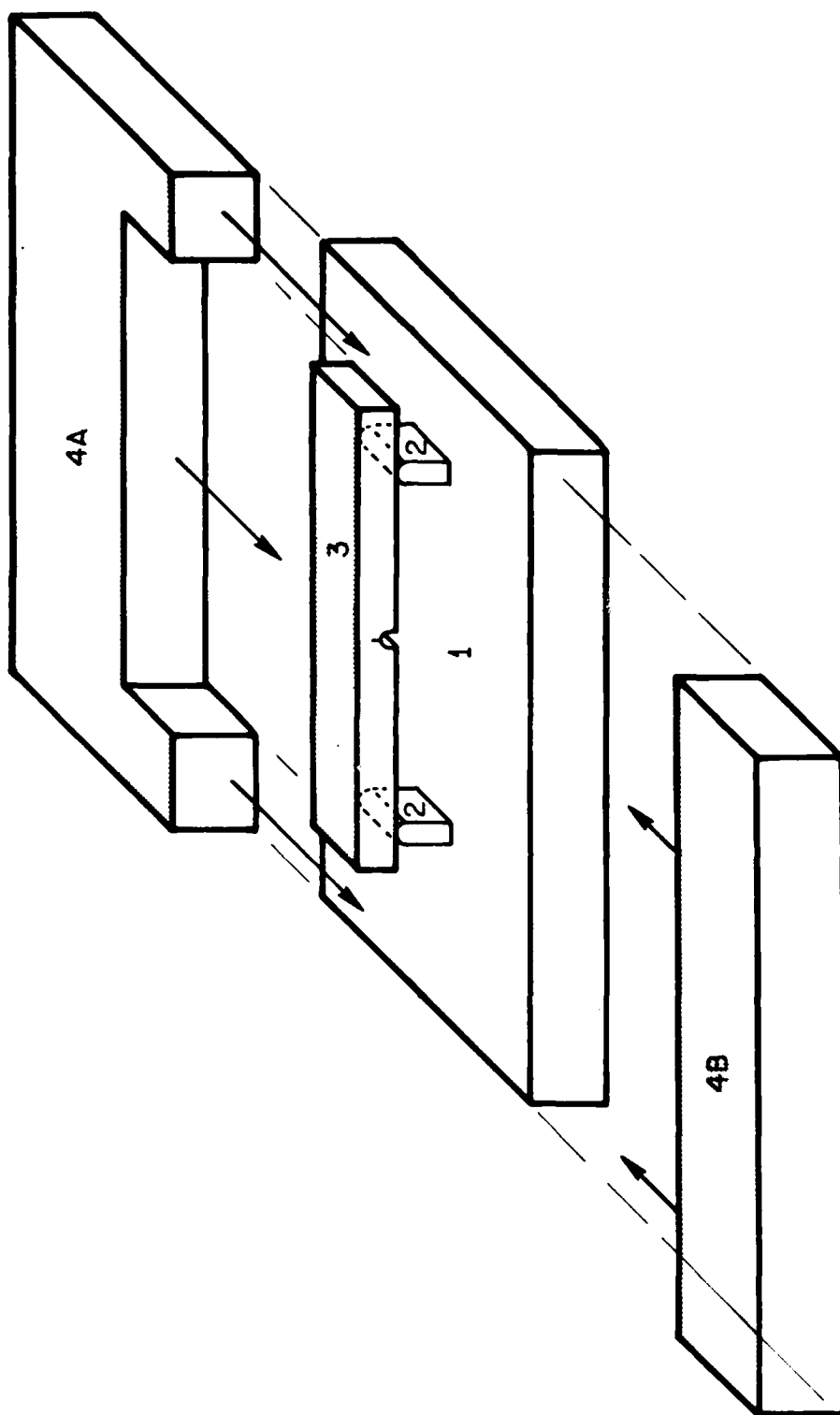
ACKNOWLEDGEMENT

FIGURE 1. SCHEMATIC REPRESENTATION OF BLAST LOADING FIXTURE

1) Base Plate   3) Specimen
2) Supports   4 a,b) Specimen encompassing plates to
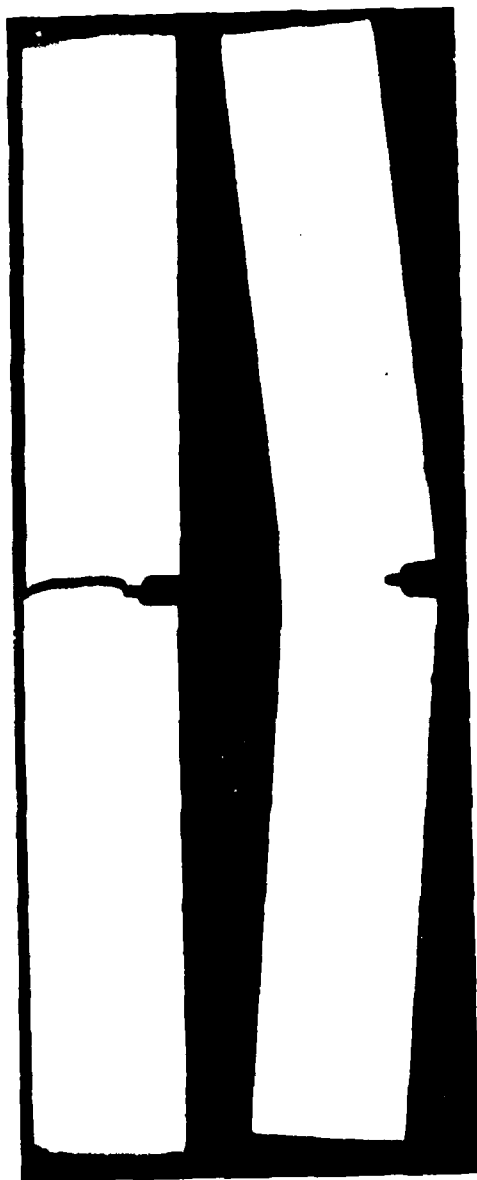   minimize gas blow by.

58

FIGURE 2. POST TEST APPEARANCE OF THE TWO PLATES SUBJECTED TO BLAST LOADING
Top - AISI 4340 Steel Specimen
Bottom - HY-130 Specimen Containing an X Type Weld.

59

AN ELASTIC-PLASTIC FRACTURE MECHANICS PREDICTION OF
FATIGUE CRACK GROWTH AT A WELDED STIFFENER IN A SHIP STRUCTURE

N.D. GHADIALI
Principal Research Scientist

T. A. WALL
Researcher

J. AHMAD
Principal Research Scientist

M. F. KANNINEN
Research Leader
BATTELLE
Columbus, Ohio 43201

EXTENDED ABSTRACT

A significant portion of all structural fractures are triggered by subcritical crack growth emanating from small initial defects in and around welds. Such growth, whether by stress corrosion or fatigue, must be affected by the presence of the thermoplastically deformed material indigenous to the welding process. The linear elastic fracture mechanics analysis techniques now in common use cannot directly treat such complications. Similarly, the elastic-plastic approaches that are now evolving, because of their limitation to deformation (reversible) plasticity, cannot readily admit residual deformation. Hence, more advanced techniques must be developed to address this problem if realistic estimates for the propensity of fracture in welded structures are to be obtained. This work-in-progress report describes a research approach for such problems. The current work is focussed on fatigue crack growth at a welded internal ring stiffener in a model of a submarine hull. However, the approach should also have broader applicability; e.g., to welded tank armor.

BACKGROUND

It has recently become possible to perform realistic elastic-thermo-plastic simulations of the welding process. As a result, it is now possible to simulate crack propagation in weld-induced residual stress and deformation fields. Drawing upon recent progress in the analysis of stable crack growth and fracture instability in the tough and ductile materials used in nuclear plants, the authors have focussed their attention on the crack tip opening displacement (CTOD) parameter as a characterizing parameter for fatigue crack growth. The specific problems studied include two crack/structure geometries - a girth welded pipe and a butt-welded plate - with three different cracking mechanisms - fatigue, stress corrosion and rapid fracture under impact loading.*

---

*These preliminary results appear in "The Numerical Simulation of Crack Growth in Weld-Induced Residual Stress Fields", by M.F. Kanninen, F.W. Brust, J. Ahmad and I.S. Abou-Sayed, Proceedings of the 28th Army Sagamore Research Conference, July, 1981.

The initial aim of this research was to critically examine the assumptions commonly used in analyzing weld cracking problems by linear elastic fracture mechanics (LEFM) techniques. This was accomplished by performing parallel sets of computations where these assumptions were and were not made. Using hypothetical (but judiciously chosen) crack growth laws based on the CTOD, it was demonstrated for both geometries considered and for all three cracking mechanisms simulated that the LEFM and the elastic-plastic predictions of crack growth behavior were considerably different. More importantly, it was shown that under these conditions design procedures based on LEFM could lead to significant non-conservatism.

Due to the lack of reliable crack growth data that could be analyzed, the above findings have thus far remained unsupported by experimental results. This work-in-progress report is aimed at amending this situation. Specifically, a prediction of the experimental data on the fatigue crack growth rate in the weld heat affected zone of an HY-80 steel model of a stiffened submarine hull (supplied by the UK Admiralty Marine Technology Establishment) is being analyzed in an effort supported by the Office of Naval Research.

APPROACH

The finite element model of the structure is shown in Figure 1. The analysis is being performed assuming axisymmetric conditions and symmetry about the weld center-line. A circumferential surface crack is assumed to exist around the periphery. The analytical procedure then consists of three main steps:

1. The residual stress field induced in the welding process is computed using an incremental thermoplastic finite element analysis procedure. This has been accomplished. The results for the normal stresses acting on the potential crack line are shown in Figure 2.

2. Crack growth is simulated by a sequential node release technique along a pre-set crack plane located in the weld-heat-affected zone, with and without the LEFM assumption. The results are then expressed in terms of crack tip opening displacement (CTOD) vs. crack length.

3. A crack growth relation based on Δ(CTOD) is then used to infer crack length as a function of time or loading history.

A load cycle in this simulation of submarine performance is taken to be one submersion and resurfacing. Hence, because the loads while submerged are compressive while the loads at the surface are likely to be small, the driving forces for fatigue cracking are simply the residual stresses themselves.

61
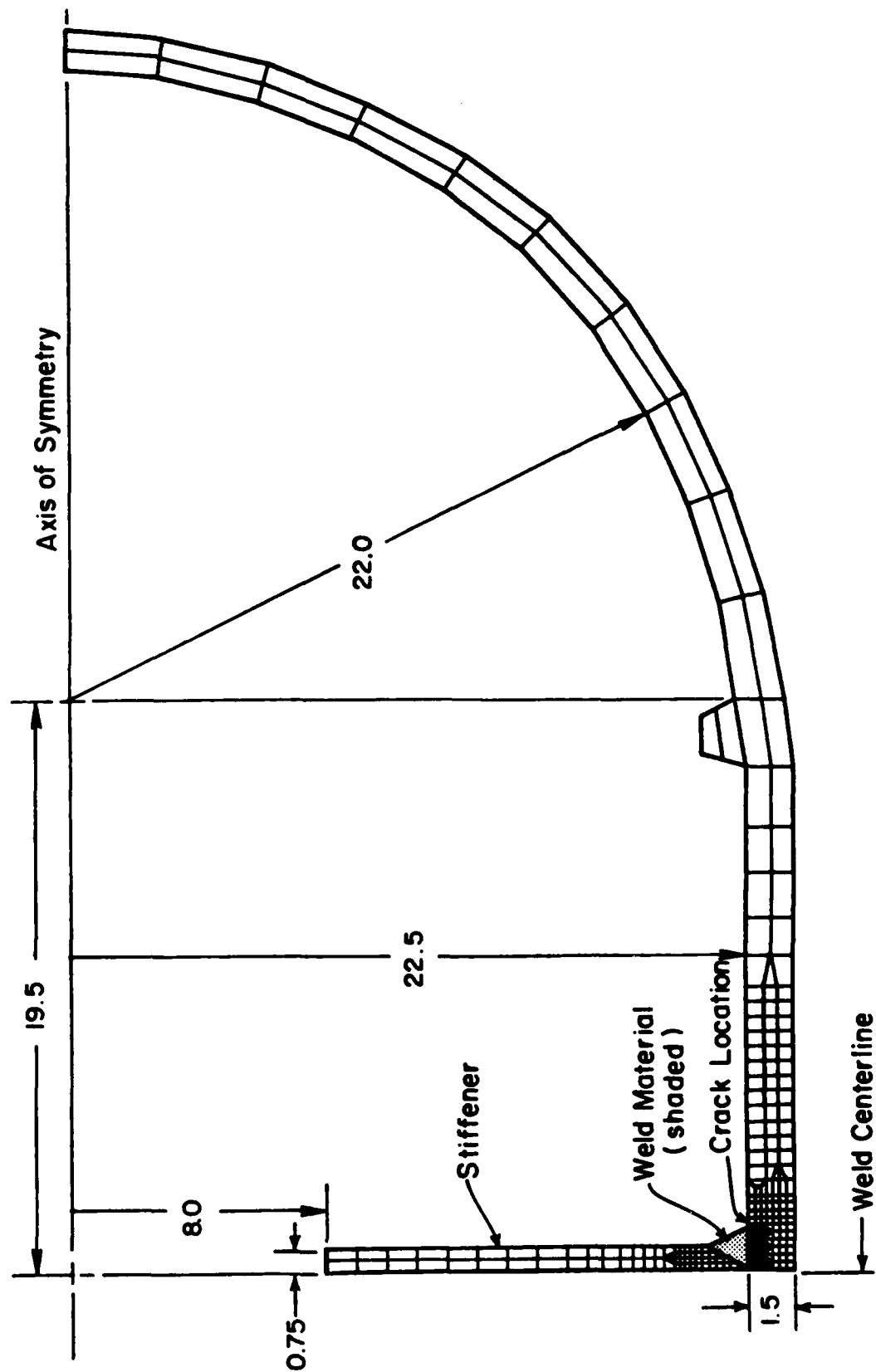
FIGURE 1. FINITE ELEMENT MODEL FOR RESIDUAL STRESS ANALYSIS OF A WELDED-ON STIFFENER (AXISYMMETRIC MODEL - ALL DIMENSIONS IN INCHES)
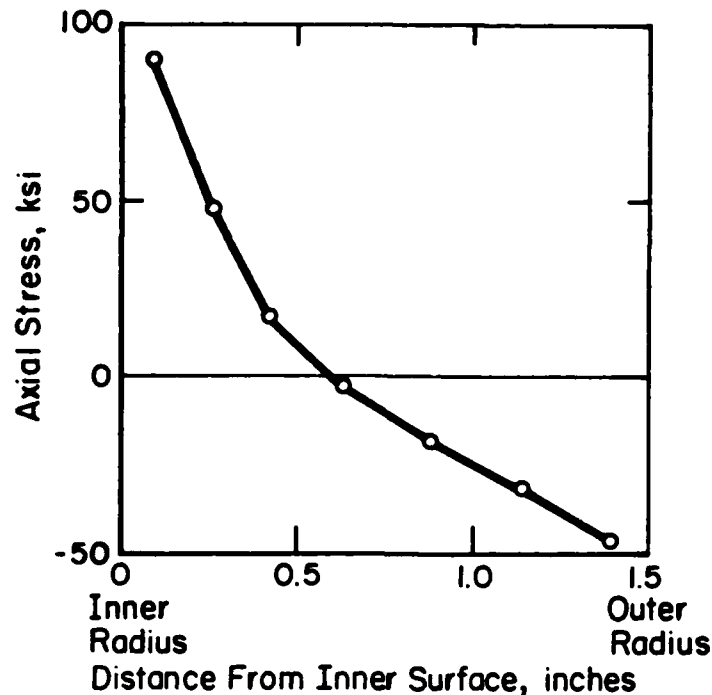
FIGURE 2. NORMAL COMPONENT OF THE RESIDUAL
STRESS ON THE PROSPECTIVE CRACK
LINE (TENSILE YIELD STRESS IS 80 KSI)

EXPECTED RESULTS

The analytical prediction and a comparison with experimentally
measured crack growth rates will be presented at the conference. This
comparison is expected to show the importance of direct consideration of
residual stresses in fatigue crack propagation and the necessity of
advanced fracture mechanics treatments. In addition, because the residual
stresses are redistributed as the crack grows, it is expected that a fatigue
crack will penetrate far deeper than the point of zero residual stress
shown in Figure 2. This has important consequences for the assessment of
the safe operating lifetime of such a structure.

ACKNOWLEDGEMENT

MODELING FOR EXPLOSIVE PRESSING

STANLEY N. SCHWANTES
Senior Principal Development Engineer
Honeywell Defense System Division
Edina, Minnesota 55436

EXTENDED ABSTRACT

Explosives for the newer high-velocity tank ammunition are being pressed into the warheads instead of being cast. This change in loading technique was brought about by the potential of the cooled cast charges to crack and create voids. The change to press loading, however, has induced problems of its own. When the high explosive is pressed into the warhead, the pressures induced sometimes cause internal components to yield, causing misalignment and degraded performance or possible safety problems. The pressing operation can also leave residual stresses in the warhead that increases overall stress during launch. Our basic problem in this effort is to understand the interactions and behavior of the warhead components during assembly and loading. Appropriate modeling techniques are being developed and verified to facilitate this understanding.

State-of-the-art finite element analysis techniques are being used to model the 120mm XM830 pressed-load warhead. These techniques are also directly applicable to future rounds. The same model can also be used to analyze in-bore loads, thus reducing modeling costs and analysis time. Model results will be compared with in-house press loading data, including anvil displacement as a function of force, strain-gage measurements, and diametral growth measurements on the warhead body. This end result will be a better understanding of warhead component interactions under severe stresses during loading and launch.

A necessary requirement for modeling explosives during final consolidation is to gather representative mechanical properties data for the explosive. Our earlier preliminary analysis will be updated in late 1982, to include physical data based on recent ARRADCOM tests of the XM830 explosive. The following sections discuss the basic model assumptions, review the model results to date, and offer conclusions and recommendations for future modeling studies.

MODEL DESCRIPTION

The objectives of the 1981 analysis were to:

o Define a finite element model of a typical large-caliber warhead and shaped-charge assembly capable of representing the non-linear interaction of components during explosive loading

o If necessary, conduct an initial analysis using approximate material properties for the explosive to check the model and the general approach.

The ANSYS finite element code is being used to model the interactions of the following components of the 120mm XM830 warhead:

o Main charge of pre-pressed HE

o   Transfer charge of pre-pressed HE
o   Copper liner
o   Plastic waveshaper
o   Steel body
o   Booster of pre-pressed HE
o   Steel booster receptacle
o   Steel anvil.

A deformed geometry plot of the model is shown in Figure 1. The anvil portion of the model is represented as a super-element (i.e., a reduced stiffness matrix) in order to reduce computer costs, it does not appear in Figure 1.

In addition to the assumptions listed in Figure 1, other significant assumptions are:

o   Density and stiffness variations in the HE, using measured data from sectioned pre-pressed main charges and transfer charges

o   For the analysis, only HE items were allowed to yield

o   A sliding coefficient of friction of 0.2 was assumed between the HE and the warhead body. Model results and recent test data show that this friction value should be increased.

Mechanical properties data for the HE used in the XM830 were not available, so the values were estimated from a similar explosive, X-0280, which consists of 95 percent RDX and 5 percent estane. The XM830 explosive is 94.5 percent RDX, 4.5 percent Montan wax, and 0.1 percent graphite.

MODEL RESULTS

The model was incrementally loaded to an equivalent anvil pressure of almost 700 bars, or about 10.15 Kpsi (70 MPa). The anvil displacement was 0.197 inches (5mm), which was too high by approximately a factor of two, as shown in Table I.

TABLE I. COMPARISON OF ANVIL DISPLACEMENTS

	Anvil Pressure (Bars)	Anvil Displacement	
		(inch)	(mm)
Model results (1981)	694	0.197	5
Honeywell Test Data	1500	0.236 to 0.275	6 to 7
Reported German Data	1500	0.118 to 0.236	3 to 6

The 1981 model analysis was terminated at this point. If better anvil displacement agreement had been obtained, the model would have been unloaded (anvil force removed) to compute residual stresses and deflections. However, despite the lack of "exact" material properties for the explosive, the behavior of the various warhead components

during pressing was characterized. Several specific results from the 1981 study are summarized below:

o A local stress concentration does occur in the main charge and the transfer charge at the edge of the plastic waveshaper. This same area in a number of warheads had minute cracks in the HE, observable on X-rays after final consolidation.

o The waveshaper does compress and store energy much like a spring.

o The explosive pellet in the warhead booster assembly, as modeled, had significant additional compression during final consolidation, which led to a density discontinuity in the adjacent web of the transfer charge.

o The coefficients of friction assumed between the warhead body and the main charge significantly affects the final density distribution in the main charge.

o The lip of the liner does not expand outward sufficiently to engage the warhead wall locking ring treads. This is primarily because the warhead wall also expands outward during pressing.

o The booster container deforms during final consolidation, thus confirming the results of sectioning a loaded warhead.

The trends predicted by the model were communicated to the warhead designers and load plant operators. The accuracy of our crack prediction in parts of the HE will improve as the material properties are better defined. The effects of piece-part tolerances on stress concentrations in the HE will also be addressed with the model. The booster pellet's predicted behavior will also change when better properties for the booster explosive (95 percent RDX, 5 percent wax) are obtained.

SMALL MODEL STUDY OF EXPLOSIVE PRESSING

A separate study was also performed using a very simple cylindrical finite element model to explore the effects of changes in non-linear material properties. Other modeling techniques and alternate material hardening laws were investigated. For example, we used the small cylindrical model to adjust the post-yield slope of the stress-strain curve for the HE material using a higher tangent modulus value. Figure 2 shows how the results from the small model determines the effect of changing Poisson's ratio for HE from 0.20 to 0.30, (0.35 was used in the larger model). Increasing Poisson's ratio from 0.20 to 0.30 increased the maximum anvil force by about 13 percent.

The small model was then unloaded (anvil force removed) to determine how the non-linear material law in the ANSYS code performed during unloading, assuming a kinematic hardening law. Both runs ($v=0.20$ and $v=0.30$) used the same five-point softening stress-strain curve that was used with the initial large model run, with maximum anvil force values well under the goal force value corresponding to 1000 bars pressure (Figure 3).

The small model was then rerun with a classical bi-linear stress-strain curve, using a tangent modulus equal to 0.105E. The anvil's maximum force increased by about 26

percent over that for the five-point stress-strain curve due to use of this tangent modulus value. This is illustrated in Figure 3. Also shown is the result of introducing a sliding friction coefficient of 0.30 between the HE and the rigid wall. This increased the maximum anvil force 42 percent.

CONCLUSIONS AND RECOMMENDATIONS

A finite element model capable of analyzing non-linear interactions of large warhead components was generated and partially verified. Explosive property data are needed to complete the model verification, though we gained insight into non-linear material properties for explosives by using the small models to conduct parametric studies. The large model has provided insight into component interactions at several interfaces in the warhead, including:

o Liner-body clearance after pressing
o Transfer charge web and booster

We are currently waiting for recent mechanical properties data for the XM830 explosives based on tests at ARRADCOM. Using the new explosive data, we will rerun the finite element model developed in 1981, compare the results with empirical assembly and loading data, and document the findings.

For future studies of explosive pressing, small models should be used to check out implementation of material properties, especially for elastic-plastic deformations, prior to starting large model studies.

In addition, more basic mechanical properties data is needed for many explosives before accurate simulations can be performed.

ACKNOWLEDGMENTS

67
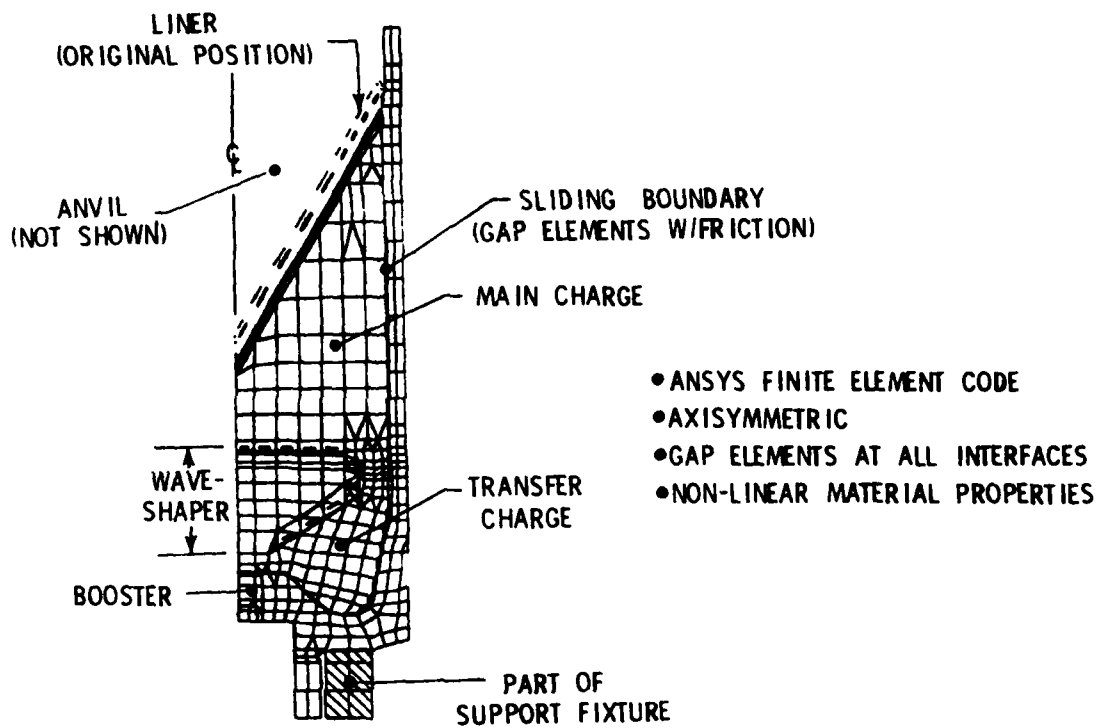
Figure 1. 120mm HEAT Warhead Press Load Model
(Deformed Geometry Plot)
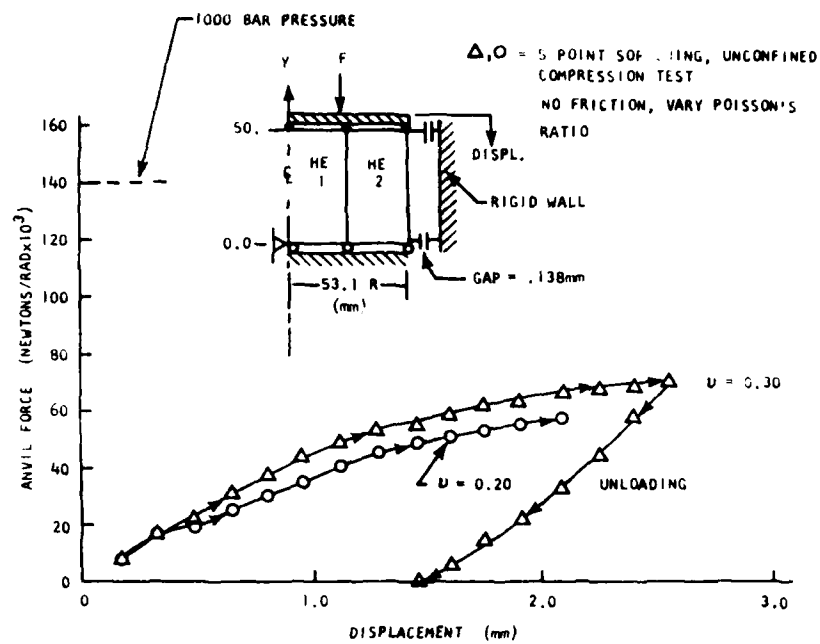
Figure 2. Compressive Force vs. Anvil Displacements

Figure 3. Compressive Force vs. Anvil Displacements
Friction and No Friction Checks

69

ACCELERATED KIscc/KIc TESTING

L. RAYMOND

METTEK Laboratories
Santa Ana, CA 92705
714-549-0671

EXTENDED ABSTRACT

The feasability of using one Charpy-sized specimen to measure both the threshold stress intensity for hydrogen assisted cracking (KIscc) and the fracture toughness (KIc) from a single specimen in less than an 8-hr test period was evaluated and shown to be extremely feasible for 4340 ESR/VAR at 43/53 HRC.

MATERIAL

An ingot of AISI 4340 AOD steel, which split and remelted by electroslag (ESR) and vacuum arc (VAR), was heat treated to two hardness levels (43 HRC and 53 HRC) by using two tempering temperatures, 340F and 900F. The steel was supplied by A. Anctil at AMMRC as blank Charpy-sized specimens. Each lot consisted of five specimens or a total of twenty specimens.
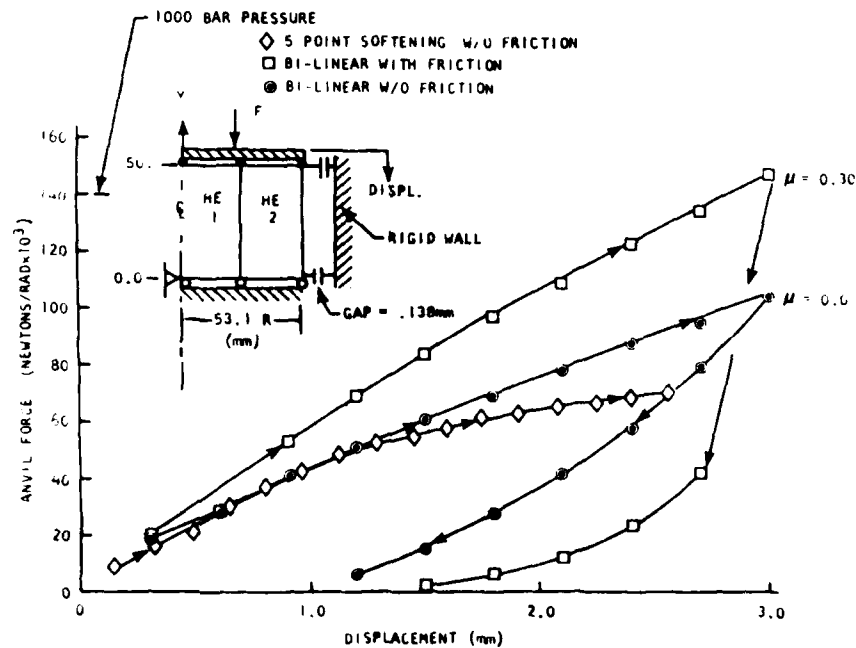
TEST OBJECTIVE

The question to be answered was, "Could the test method developed by the author for high-toughness ship steels be adapted to high-strength ballistically tolerant steels to not only measure KIscc but also KIc?" Other test methods had been used to rate the relative susceptibility of the same steel in the same conditions but none gave quantitative results that can be incorporated as design parameters. The other test methods only provided relative measurements and their results can only be used for comparative purposes.

APPROACH

Two samples from each lot were tested per ASTM STD E399-81 for fracture toughness; one in a 3-pt bend fixture with an Instron test machine and the other in a specially designed 4-pt loading frame. The 53 HRC specimens provided valid fracture toughness measurements; the 43 HRC specimens were invalid per ASTM STD E399-81. While the tests were conducted, both load-line-displacement and crack-opening-displacement were monitored to

70

provide elastic-plastic J-intergral and COD estimates of fracture toughness for the 43 HRC specimens. Comparisons are made among the various methods.

Three samples from each lot were heavily side-grooved in addition to having a sharper notch than the 10-mils called for in ASTM STD E23. One sample was loaded to fracture in air and the remaining two samples were tested by the previously reported step-load KIscc test method. After the initiation load was recorded for KIscc measurement, the specimens were monitored to various amounts of hydrogen assisted slow crack growth in the 3.5 percent salt water solution while cathodically polarized at -1.0V vs SCE to produce hydrogen at the specimen surface. As soon as the test was terminated, the specimens were baked for 24 hrs at 300F. Then the specimens were re-installed in the load frame and tested to fracture in air.

RESULTS

The testing is incompleted but the data reduction is still in progress. Preliminary results suggest an excellent correlation between several parameters tested by the various methods.

1. KIc or fracture toughness measurements per ASTM E399 3-pt bend are compared to results with (1) 4-pt bend on fatigue precracked specimens with $Bn/B=1$ & $a/W=0.5$, (2) notched $Bn/B=0.4$ & $a/W=0.2$ and (3) hydrogen stress assisted cracked-specimens with $Bn/B=0.4$ & a/W ranging from 0.22 to 0.70, both for linear elastic and elastic-plastic analysis by COD, and J-intergral, and equivalent energy techniques.

2. KIscc is measured and compared to literature values. The ranking of the samples with regard to hydrogen embrittlement susceptibility is compared to other relative test methods measurements.

3. The ability to obtain the ratio of KIscc/KIc from one sample by the ratio of initiation load for H-cracking and fracture is demonstrated.

CONCLUSIONS

An accelerated KIscc/KIc test method appears to be feasible for high strength steels. The results appear to be internally consisted with analyses from several approaches. Other than being an accelerated test, (1) the test specimen requires only enough material for modified-Charpy specimens (2) the load is applied manually, (3) machine-notched specimens are used instead of

71

fatigue precracked, and (4) the test can be completed in 8-hrs even in measuring KIscc; thereby providing many other factors that will lower the cost of fracture toughness testing.
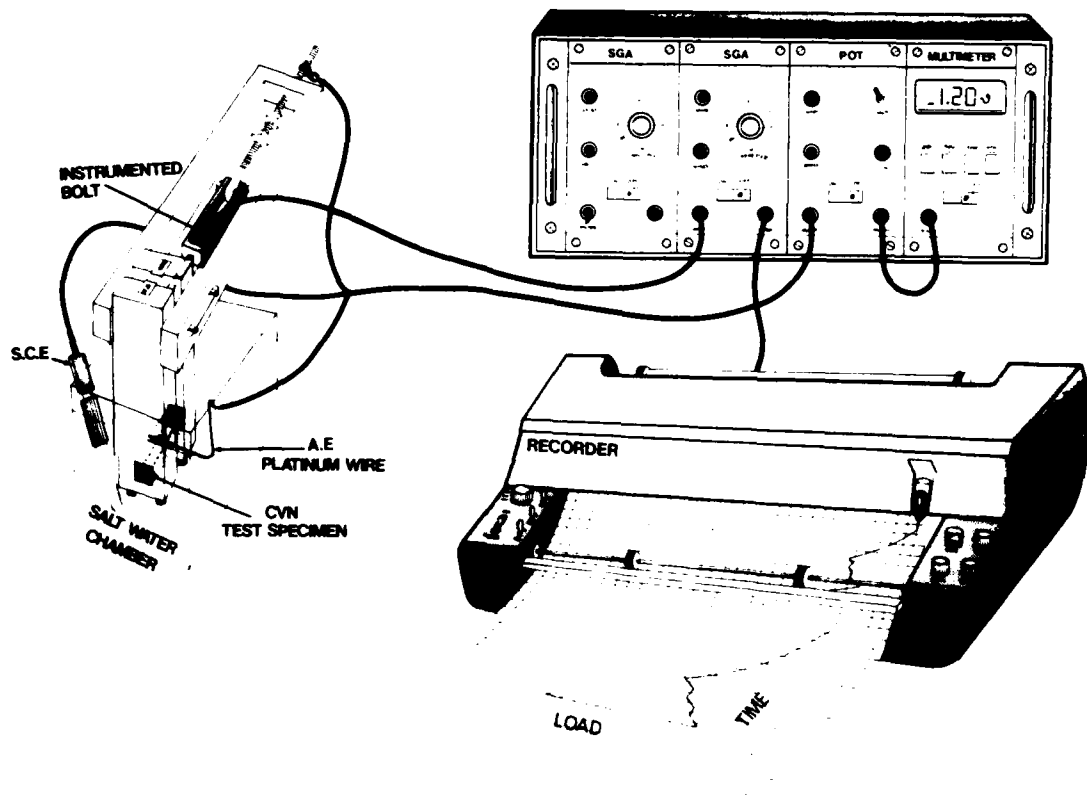
Miniature/Modular fracture mechanics lab for accelerated KIscc/KIc testing.

STUDY OF FAILURE STRENGTH OF ADVANCED PROJECTILES
AFTER YIELDING AND PLASTIC FLOW

J. ADACHI
Research Team Leader
Army Materials and Mechanics Research Center
Watertown, MA   02172

W. FOSTER
Engineering Technician
Army Materials and Mechanics Research Center
Watertown, MA   02172

T. E. LEE
Mechanical Engineer
ARRADCOM
Dover, NJ

ABSTRACT

1. INTRODUCTION

During its brief launch experience an artillery projectile is subjected to a sequence of major loads each of which and the cumulative damaging effect of which the projectile must successfully sustain: These successive major loads include a possible initial large torsional impulse; the high acceleration, torsional and pressure forces at peak pressure and the sudden negative acceleration which occurs at barrel exit as the propelling gas pressure suddenly drops off.

For most projectiles the structural case is very simple, the stresses developed are generally moderate and elastic, and the necessary and desired reliability levels are easily attained and simple to document.

However, in some of the more advanced projectiles unusual structural and material problems arise as a consequence of the complicated structural geometrics; the resulting complex and uncertainly known stress conditions; the little known materials behavior under these complex stress conditions and the need for a level of reliability that is not only high but that is also supported by careful, thorough and well-documented analysis prerequisite for defense of the reliability of the system before review groups.

A most unusual problem currently under study involves these conditions with the added complexity of a material (6-6-2 Ti), not extremely tough at best, that in critical regions may undergo compressive yield and significant plastic flow during the peak acceleration period of the launch. The unknown effect of the yielding and plastic flow on the tensile properties of the material and therefore the ability of the material to sustain the major stress reversal (from compression to tension) at barrel exit is a major concern. The effect would almost certainly involve Bauschinger effect which, combined with residual tensile stresses, might reduce the tensile yield rupture strength under the barrel exit

73

tensile load to a less than acceptable level. Also, the effect of compressive yielding and plastic flow on the fracture toughness of the material is unknown. Both of these effects involve phenomenology concerning which general understanding is meager and useful information for most materials does not exist. Therefore, resolution of this problem requires complete study starting from the exploratory and basic research levels and carried through continuously to successful development of fielded hardware.

Of almost equal urgency are other facets of the structural reliability problem that are peculiar to advanced projectiles. Continuously measured values of 3-D elastic-plastic strains in critical areas are needed to supplement stress analyses and provide accurate definition of 3-D stress states including the cumulative damage effects. Also, measured values of failure strengths are needed to define margins of safety and reliability levels under each load type in the launch sequence including the cumulative damage effects of earlier loads.

These problems are presently being studied in connection with the XM-785 155 mm nuclear projectile. How they are being studied is the subject of this presentation.

2. DESCRIPTION OF PROGRAM

a. Test Models

The study is making use of used hardware to reduce the cost. On hand are nineteen parachute-recovered projectile rear body components (Fig. 1, Fig. 2), all of which have sustained one firing at some pressure level. The critical area in the region of the splined joint tool run-out groove is intact on most of these components. Damage appears to be limited to superficial scratches and shallow grooving on the outer surface except on two projectiles fired at the highest zones (highest pressures) which have sustained localized damage on the inside in the form of a shearing off of a supporting lip.

These components will be used as test models for ultimate strength tests and as a material source for materials properties test specimens. At this writing, exact plans are being worked out for cutting up the components and extracting test specimens for the following series of tests.

b. Determination of Fracture Toughness After Compressive Yield and Plastic Flow

This test will require the fabrication of a specimen blank or other configuration which can be loaded through the compressive yield and plastic strain experience expected in the critical area of the projectile during the launch firing. Following this preconditioning, it is necessary to be able to fabricate a fracture toughness specimen from the preconditioned blank with the specimen crack located in material in the same condition as the material in the critical area of the actual projectile.

It appears that small plane strain fracture toughness bend specimens, Fig. 3, with crack oriented either circumferentially (preferred) or radially (acceptable)

74

can be cut from the lower cylindrical part of the rear components. Blanks for
three specimens will be cut, strain gaged, and preconditioned by loading in com-
bined compression and bending to produce the desired yielding and plastic strain
at the location of the tip of the crack. Nine specimens to provide three replicates
at each of three strength levels representing the spread of strength in the nine-
teen projectile bodies will be fabricated, precondition loaded, and tested for
fracture toughness. Three control specimens at each strength level will be
fabricated and tested without load preconditioning to represent as-fabricated
fracture toughness.

Comparison of the results of this series of tests should reveal the existence,
magnitude, and seriousness of the effect of yielding and plastic flow on the
fracture toughness of the high strength 6-6-2 titanium alloy.

c. Bauschinger Effect in 6-6-2 Titanium Alloy

Also from the recovered rear body components a number of Bauschinger test
specimens will be machined as shown in Fig. 4. Series of these will be tested
to cover the range of compression yield and plastic strain levels that is expected
in the projectiles during launch. Test series for each of three strength levels
of material will be performed. Control specimens at each strength level will be
tested three in compression-only to failure and three in tension-only to failure.
The results of these tests will reveal the magnitude of the Bauschinger effect
on the material and the resulting failure strength level as compared to the
ordinary uniaxial strength of the material.

d. Elastic-Plastic Strains and Failure Strength of Joint Sections of Projectile

The critical section of the projectile appears to be in the splined joint
between the rear body or rocket motor (Figs. 1 and 2) and the forward body. Test
specimens will be fabricated using the recovered components, strain gaged at
critical points and tested under various loads and load sequences as shown in
Fig. 5. The strain data will provide magnitudes of stresses and strains in the
critical zone which will be used to load or precondition load the test specimens
described earlier. Failure load results will demonstrate margins of safety for
each major load in the launch load sequences and all the possible load sequences.

e. Charpy Impact Toughness

In addition to the fracture toughness tests, paralleling Charpy impact
specimens will be fabricated, load preconditioned and tested. These results will
be used to determine if compressive yielding and plastic strain effects on the
toughness of the material can be detected equally well by Charpy as by fracture
toughness testing. In addition, close correlations between Charpy impact and
fracture toughness will allow the more confident use of Charpy tests for process
and quality control in place of the more complicated and expensive fracture
toughness test.

3. CONCLUSION

This study is only a portion of the research activities being carried out for the XM-785 system. Other critical regions of the projectile are receiving or will receive similar treatment to insure that the entire projectile will demonstrate the necessary level of reliability. The specific approaches and procedures described above are subject to change as the program progresses and as more and better information on the behavior of the structure and material under load becomes available.
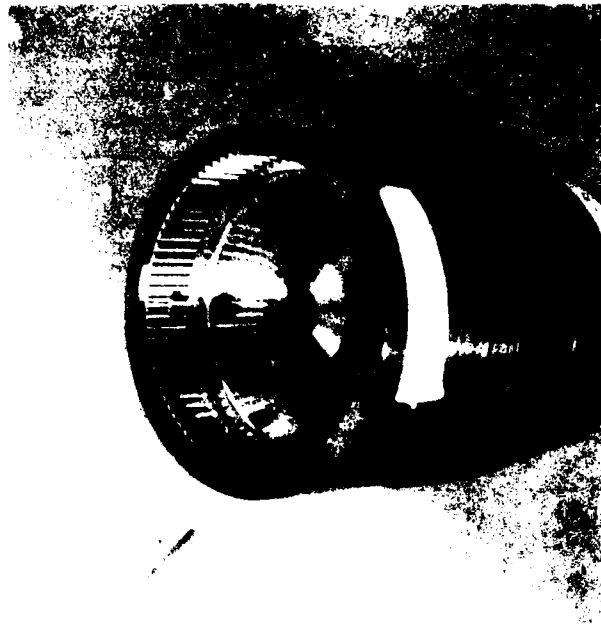
FIG. 1 - REAR BODY XM-785 SHOWING SPLINED JOINT

FIG. 2 - ROCKET MOTOR XM-785 SHOWING SPLINED JOINT AND BULKHEAD

1. DIMENSIONS IN INCHES UNLESS OTHERWISE NOTED.

2. (A) SURFACES TO BE PER-PENDICULAR AND PARALLEL AS APPLICABLE TO WITHIN .001W TIR.

3. INCLUDED ANGLE AND RADIUS OF NOTCH TO BE DETERMINED BY ENGINEER.

4. LENGTH OF FATIGUE CRACK SHALL NOT BE LESS THAN 5 PERCENT OF THE OVERALL LENGTH (A_1 + A_2), AND NOT LESS THAN .05.

5. CRACK STARTER TO BE PER-PENDICULAR TO SPECIMEN LENGTH AND THICKNESS TO WITHIN $\pm 2°$.

TYPE	A_1	A_2	B	H	K
FT 1	2.05(W) MIN	2.05(W) MIN	$\frac{(W)}{2}$	.250 - .200	.05 - .06

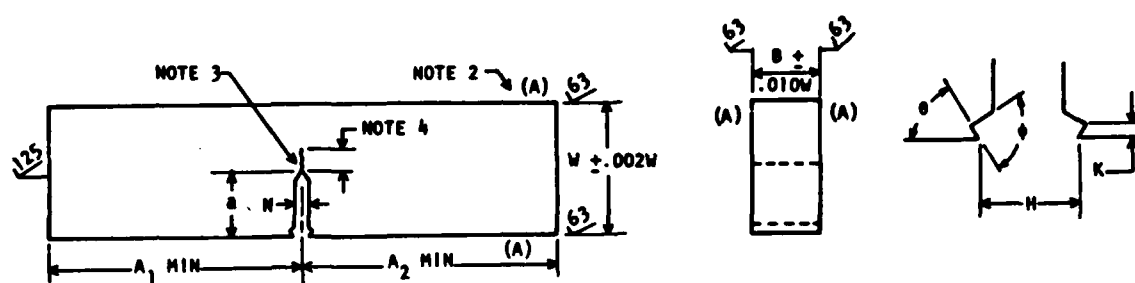| TYPE	N	W	a	ϕ	θ
FT 1	.05(W)		.45 - .55(W)	$0 \le \phi \le 90°$	$45° \le \theta \le 60°$

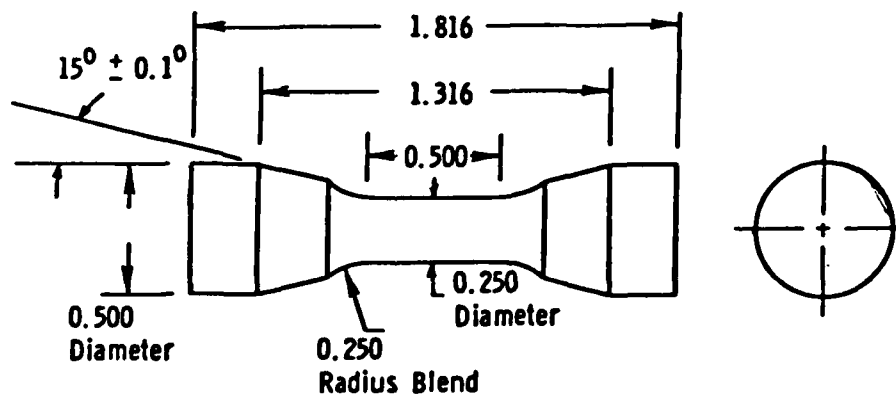FIG. 3 - PLANE STRAIN FRACTURE TOUGHNESS BEND SPECIMEN

FIG. 4 - BAUSCHINGER EFFECT SPECIMEN

78

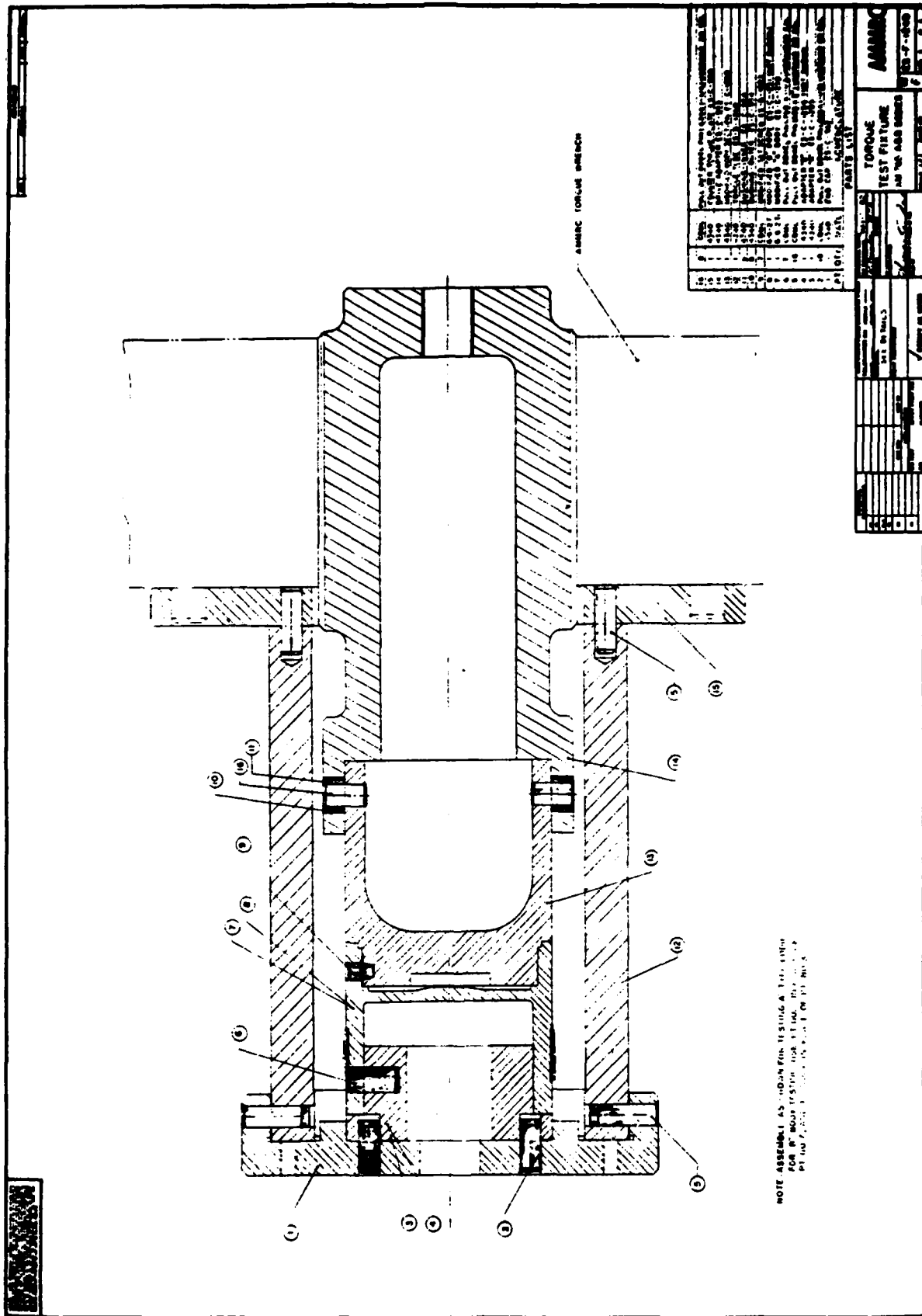FIG. 5a - TORSION TEST FIXTURE FOR XM-785 BODIES
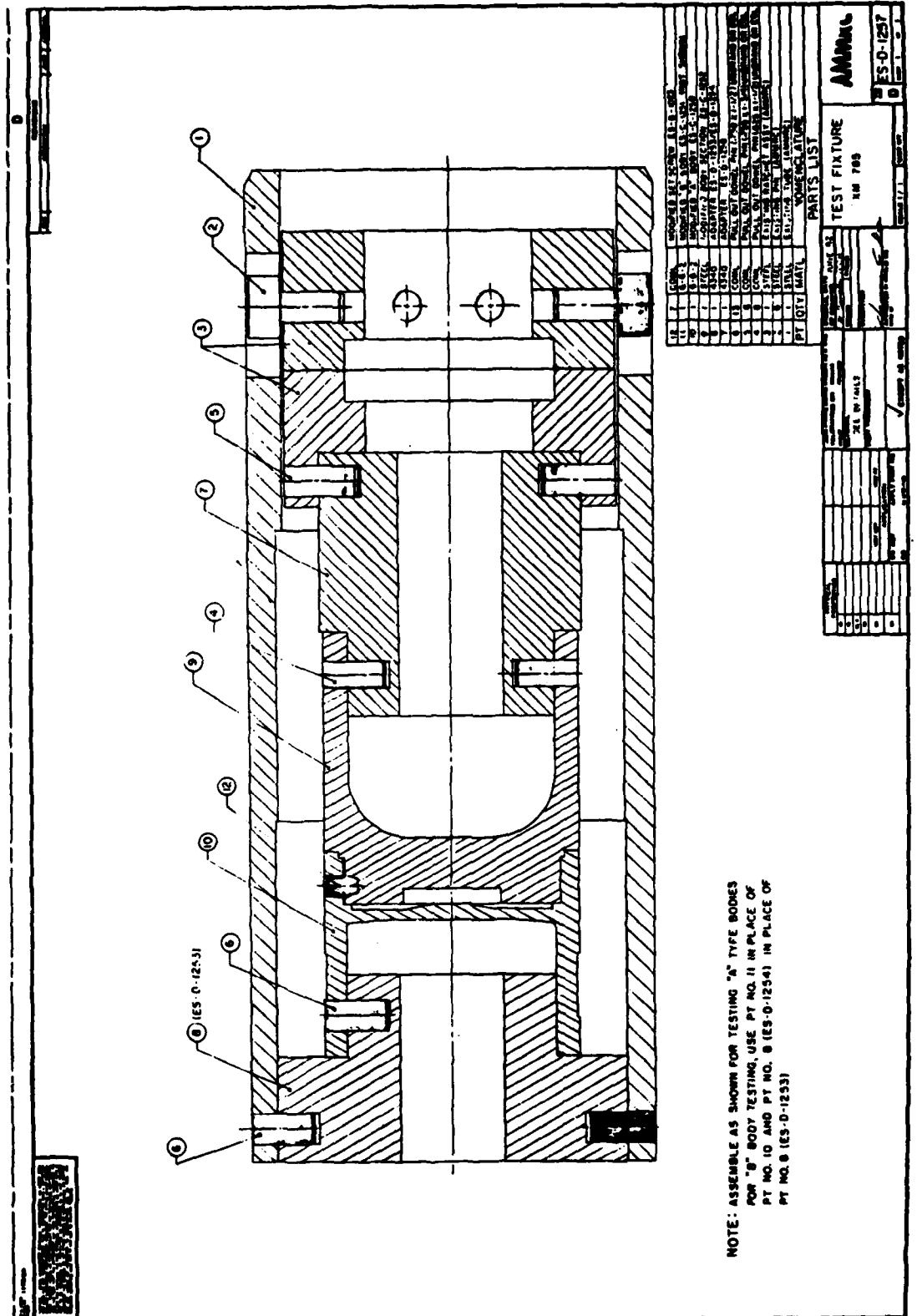
FIG. 5b - COMBINED TORSION-COMPRESSION TEST FIXTURE FOR XM-785 BODIES

NOTE: ASSEMBLE AS SHOWN FOR TESTING "A" TYPE BODIES
FOR "B" BODY TESTING, USE PT NO. 11 IN PLACE OF
PT NO. 10 AND PT NO. 8 (ES-D-1254) IN PLACE OF
PT NO. 8 (ES-D-1253)

AUTHOR INDEX

Adachi, J.	Army Materials and Mechanics Research Center	Watertown, MA	20,73
Ahmad, J.	Battelle Columbus Laboratories	Columbus, OH	56,60
Anastasi, R.	Army Materials and Mechancis Research Center	Watertown, MA	20
Arora, J. S.	The University of Iowa	Iowa City, IA	5
Barnes, C. R.	Battelle Columbus Laboratories	Columbus, OH	56
Barsoum, R.	Army Materials and Mechanics Research Center	Watertown, MA	1
Belegunda, A. D.	The University of Iowa	Iowa City, IA	5
Bowie, O. L.	Army Materials and Mechanics Research Center	Watertown, MA	31
Clark, Jr., W. G.	Westinghouse R&D Center	Pittsburgh, PA	43,54
Chiang, F-P	Moire Stress, Incorporated	Port Jefferson, NY	20
Cowles, B. A.	Pratt & Whitney Aircraft Group	W. Palm Beach, FL	37
Faster, W.	Army Materials and Mechanics Research Center	Watertown, MA	73
Freese, C. E.	Army Materials and Mechanics Research Center	Watertown, MA	31
Ghadiali, N. D.	Battelle Columbus Laboratories	Columbus, OH	60
Greenspan, J.	Army Materials and Mechanics Research Center	Watertown, MA	44
Gupta, A. D.	Army Armament R&D Command	Aberdeen, MD	51
Hubble, W. S.	EnerGroup, Incorporated	Portland, ME	55
Kanninen, M. F.	Battelle Columbus Laboratories	Columbus, OH	56,60
Kassir, M. K.	City University of New York	New York, NY	29
Lee, T. E.	Army Armament R&D Command	Dover, NJ	73
Most, I. G.	EnerGroup, Incorporated	Portland, ME	55
Nguyen, D. T.	Northeastern University	Boston, MA	5
Penty, R. A.	EnerGroup, Incorporated	Portland, ME	55
Peters, J. R.	Army Materials and Mechanics Research Center	Watertown, MA	36
Raymond, L.	METTEK Laboratories	Santa Ana, CA	70
Schwantes, S. N.	Honeywell Defense Systems Div.	Edina, MN	64
Tracey, D. M.	Army Materials and Mechanics Research Center	Watertown, MA	31
Wall, T. A.	Battelle Columbus Laboratories	Columbus, OH	60
Warren, J. R.	Pratt & Whitney Aircraft Group	W. Palm Beach, FL	37
Wisniewski, H. L.	Army Armaments R&D Command	Aberdeen, MD	51
Wolman, M. R.	EnerGroup, Incorporated	Portland, ME	55